A fusion peptide in preS1 and the human protein-disulfide isomerase ERp57 are involved in HBV membrane fusion process

Jimena Pérez-Vargas, Elin Teppa, Fouzia Amirache, Bertrand Boson, Rémi Pereira de Oliveira, Christophe Combet, Anja Böckmann, Floriane Fusil, Natalia Freitas, Alessandra Carbone, et al.

▶ **To cite this version:**

Jimena Pérez-Vargas, Elin Teppa, Fouzia Amirache, Bertrand Boson, Rémi Pereira de Oliveira, et al.. A fusion peptide in preS1 and the human protein-disulfide isomerase ERp57 are involved in HBV membrane fusion process. eLife, 2021, 10, 10.7554/eLife.64507 . hal-03275938

HAL Id: hal-03275938
https://hal.sorbonne-universite.fr/hal-03275938

Submitted on 1 Jul 2021

HAL is a multi-disciplinary open access archive for the deposit and dissemination of scientific research documents, whether they are published or not. The documents may come from teaching and research institutions in France or abroad, or from public or private research centers.

L'archive ouverte pluridisciplinaire **HAL**, est destinée au dépôt et à la diffusion de documents scientifiques de niveau recherche, publiés ou non, émanant des établissements d'enseignement et de recherche français ou étrangers, des laboratoires publics ou privés.

A fusion peptide in preS1 and the human protein-disulfide isomerase ERp57 are involved in hepatitis B virus membrane fusion process

Authors:

Jimena Pérez-Vargas[1,*], Elin Teppa[2,3,*], Fouzia Amirache[1], Bertrand Boson[1], Rémi Pereira de Oliveira[1], Christophe Combet[4], Anja Böckmann[5], Floriane Fusil[1], Natalia Freitas[1,**], Alessandra Carbone[2,**,$] and François-Loïc Cosset[1,**,$]

Affiliations:

[1]CIRI – Centre International de Recherche en Infectiologie, Univ Lyon, Université Claude Bernard Lyon 1, Inserm, U1111, CNRS, UMR5308, ENS Lyon, 46 allée d'Italie, F-69007, Lyon, France.

[2]Sorbonne Université, CNRS, IBPS, Laboratoire de Biologie Computationnelle et Quantitative (LCQB) - UMR 7238, 4 place Jussieu, 75005 Paris, France.

[3]Sorbonne Université, Institut des Sciences du Calcul et des Données (ISCD), 4 place Jussieu, 75005 Paris, France.

[4]Cancer Research Center of Lyon (CRCL), UMR Inserm 1052 - CNRS 5286 mixte CLB – UCBL1, F-69008 Lyon, France.

[5]Molecular Microbiology and Structural Biochemistry, UMR5086 CNRS-Université Lyon 1, 7 passage du Vercors, 69367 Lyon, France.

*These authors contributed equally to the work.

**These senior authors contributed equally to the work.

[$]Corresponding authors: Address: ENS Lyon, 46 allée d'Italie, F-69007, Lyon, France ; tel: +33472728732; e-mail: flcosset@ens-lyon.fr

Address: LCQB, Sorbonne Université, 4 place Jussieu, 75005 Paris, France; tel: +33144277345; e-mail: alessandra.carbone@sorbonne-universite.fr

Short title:

Hepatitis B virus membrane fusion determinants

Summary

Cell entry of enveloped viruses relies on the fusion between the viral and plasma or endosomal membranes, through a mechanism that is triggered by a cellular signal. Here we used a combination of computational and experimental approaches to unravel the main determinants of hepatitis B virus (HBV) membrane fusion process. We discovered that ERp57 is a host factor critically involved in triggering HBV fusion and infection. Then, through modelling approaches, we uncovered a putative allosteric cross-strand disulfide (CSD) bond in the HBV S glycoprotein and we demonstrate that its stabilization could prevent membrane fusion. Finally, we identified and characterized a potential fusion peptide in the preS1 domain of the HBV L glycoprotein. These results underscore a membrane fusion mechanism that could be triggered by ERp57, allowing a thiol/disulfide exchange reaction to occur and regulate isomerization of a critical CSD, which ultimately leads to the exposition of the fusion peptide.

Introduction

Hepatitis B is a major public health problem; it affects over 250 million people worldwide and 850,000 deaths occur each year as a result of hepatitis B complications (WHO, March 2015). The structure of its etiological agent, the hepatitis B virus (HBV), features a nucleocapsid that is surrounded by a lipid bilayer containing the envelope glycoproteins (GPs) designated as the small (S), medium (M) and large (L), which are the product of a single open reading frame. They share the C-terminal S-domain that contains four putative transmembrane domains. The L and M proteins have N-terminal extensions (preS1/prS2 and preS2, respectively) that mediate diverse functions in nucleocapsid binding and receptor recognition (Baumert et al., 2014). The first 2-75 amino acids sequence of the preS1 domain of the L protein (Blanchet and Sureau, 2007; Bremer et al., 2011; Le Seyec et al., 1999) and the antigenic loop (AGL) of the S domain (Le Duff et al., 2009; Salisse and Sureau, 2009; Schulze et al., 2007) have been identified as essential determinants for infectivity of HBV and hepatitis delta virus (HDV).

Entry of enveloped viruses into cells can be defined as the sequence of events occurring from the attachment of the virus to the host cell until the release of the genome in the cytoplasm, *via* fusion between viral and cellular membrane. Like for most enveloped viruses, HBV entry into cells is a finely regulated and complex process consisting in different steps, in which several viral and cellular factors are involved. Its first step involves low-affinity binding to heparan sulfates proteoglycans (HSPGs) residing on the hepatocytes' surface (Leistner et al., 2008; Schulze et al., 2007). This attachment is mediated by the preS1 region of the L protein and/or the antigenic loop of the S protein (Ni et al., 2014; Schulze et al., 2007). Afterwards, the virus interacts with its high-affinity receptor, the sodium taurocholate-cotransporting polypeptide (NTCP) (Ni et al., 2014; Yan et al., 2012) through the amino-terminal end of the L protein preS1 domain (Glebe et al., 2005a; Gripon et al., 2005; Yan et al., 2012). NTCP is an integral membrane protein, expressed at the basolateral membrane of hepatocytes, which explains the tropism of HBV for the liver.

The post-binding entry steps of HBV occur through endocytosis; however, the exact mechanism is still unclear and somehow controversial. One early study showed that HBV in HepaRG cells is internalized *via* caveolin-mediated endocytosis (Macovei et al., 2010). Nevertheless, inhibition of caveolin-mediated endocytosis or silencing of caveolin-1 did not impair HBV infection in Tupaia hepatocytes (Bremer et al., 2009) or in HepaG2-NTCP cells (Herrscher et al., 2020). Contrastingly, several other studies presented evidence that HBV endocytosis is clathrin-dependent (Herrscher et al., 2020; Huang et al., 2012; Umetsu et al., 2018). Recent studies reported that HBV infection of HepaRG cells depends on Rab5 and Rab7 (Macovei et al., 2013), which are GTPases involved in the biogenesis of endosomes, and that the epidermal growth factor receptor (EGFr) is a host-entry cofactor that interacts with NTCP and mediates HBV internalization (Iwamoto et al., 2019). These findings support

the hypothesis that HBV is transported from early to mature endosomes. After the early endosome stage, translocation is associated with a gradually decreasing pH, from about 6.2 in early endosomes to close to 5.5 in late endosomes, which allows fusion of many enveloped viruses with the endosomal membrane. However, in the case of HBV, pharmacological agents that raise or neutralize the pH in the endocytic pathway do not affect infection (Macovei et al., 2010, 2013; Rigg and Schaller, 1992). Furthermore, treatment with protease inhibitors have no effect on infection (Macovei et al., 2013), suggesting that HBV transport into the degradative branch of the endocytic pathway is not required *per se* to initiate this process.

Virus entry by membrane fusion involves interactions between viral fusion proteins and host receptors, which results in conformational changes of the virus envelope proteins. However, the molecular determinants and mechanism of membrane fusion of HBV remain to be defined. Previous results indicated the essential role of the cysteine residues of the antigenic loop, as shown by the reduction of virus entry levels by inhibitors of thiol/disulfide exchange reaction (Abou-Jaoudé and Sureau, 2007), hence suggesting a redox state responsible for conformational changes that can have a role during the fusion step.

Here, using a combination of computational and experimental approaches, we sought to better understand how HBV induces the fusion of its lipid membrane with that of the infected cell. Specifically, using a coevolution analysis of HBV GPs and molecular modelling combined with experimental investigations *ex vivo* in molecular virology and *in vivo* in liver humanized mice, we provide evidence that the mechanism triggering HBV membrane fusion involves ERp57, a cellular protein disulfide isomerase. Furthermore, our results highlight the role of specific cysteines in the AGL determinant and well as a sequence (aa 48 to 66) in the preS1 determinant that could ultimately act as a fusion peptide mediating HBV membrane fusion.

Results

HBV membrane fusion is independent of acid pH and receptor expression. To investigate the fusion activation mechanism and to identify the fusion determinants of HBV, we designed a cell-cell fusion assay whereby Huh7 “donor” cells, expressing a luciferase reporter gene under control of the HIV-1 promoter, were co-cultured with either Huh7-tat or Huh7-NTCP-tat “indicator” cells, expressing the HIV-1 transactivator of transcription (Tat) protein, which induces luciferase expression only in fused donor and indicator cells (Lavillette et al., 2007). We transfected donor cells with pT7HB2.7 (Sureau et al., 1994), an expression plasmid encoding the wild-type HBV glycoproteins L, M and S. The transfected donor cells where then co-cultivated with Huh7-tat or Huh7-NTCP-tat indicator cells for 1 day. The medium of the co-cultures was then acidified at pH4 for 3 min to trigger fusion and the

next day, the luciferase activity in the lysates of co-cultured cells was measured as a read-out of membrane fusion (Figure 1A). The GPs of vesicular stomatitis virus (VSV) or of Crimean-Congo hemorrhagic fever virus (CCHFV) were used as controls for viruses that need acidic pH to promote membrane fusion. We found that HBV GPs induced similar levels of fusion in co-cultures that were exposed to either acidic or neutral pH, as well as in co-cultures lacking or expressing the NTCP receptor (Figure 1A; see raw data in Figure 1-figure supplement 1). Since HBV entry requires HSPG to mediate the capture of its viral particles through HBsAg (Leistner et al., 2008; Schulze et al., 2007), we addressed whether blocking of HBsAg/HSPG interaction could inhibit cell-cell fusion using heparin as competitor. Yet, while the applied doses of heparin could prevent cell-free entry, as shown previously (Schulze et al., 2007), addition of soluble heparin to the co-cultures did not prevent HBsAg mediated fusion, whether the indicator cells expressed or not NTCP (Figure 1B). We confirmed these results by using CHO and CHO-pgsB618 (Richard et al., 1995) cells as donor and/or indicator cells. While both cell types do not express NTCP, only the former expresses HSPGs. We found that cell-cell fusion could be detected for either indicator cell type to the same extent as for Huh7 cells (Figure 1C). Altogether, these results indicated that cell-cell fusion mediated by HBV GPs is independent of acid pH and requires neither HSPG nor NTCP receptor, which underscores an alternative fusion trigger.

The preS1 domain of HBsAg harbors a critical determinant of membrane fusion. The L, M and S GPs of HBV are produced by a single open reading frame and share a common C-terminal S-domain. M and L proteins harbor additional N-terminal extensions (preS2 and preS1/preS2, respectively), with preS1 harboring the NTCP-binding determinant (Glebe et al., 2005b; Gripon et al., 2005). Noteworthy, the fusion determinants of HBV GPs and, particularly, the fusion peptide that could induce merging of viral and endosomal membranes has not yet been functionally identified in infection or cell-cell fusion assays.

First, to address which GP is responsible for HBV membrane fusion, we evaluated the role of either proteins in cell-cell fusion assays (Figure 1D). Huh7 cells were transfected with plasmids encoding wt HBV GPs, *i.e.*, L, M and S (pT7HB2.7 plasmid), *vs*. only L, M or S (using pCiL, pCiM and pCiS plasmids, respectively) (Komla-Soukha and Sureau, 2006). To analyze the expression of either protein at the cell surface, transfected cells were labeled with sulfo-NHS-SS-biotin, a chemical compound that is unable to penetrate biological membranes. After lysis and immuno-precipitation of biotinylated proteins, we found that the individually expressed L, M or S proteins were detected at similar levels as compared to HBV GPs (L, M and S) expressed simultaneously, as in cells transfected with the wt pT7HB2.7 plasmid (Figure 1E, 1F). Then, to determine the fusion activity of either protein, we performed cell-cell fusion assays as described above. We found that none of the L, M or S proteins expressed alone were able to induce membrane fusion (Figure 1D). Furthermore, when we tested the pT7HB2.7Mless plasmid, which induces co-expression of S and L only (“noM” in Figure 1D-1F), we

detected a cell-cell fusion activity at the same level than for wt HBV GPs (Figure 1D). This indicated that M is not necessary for membrane fusion, in agreement with previous results (Ni et al., 2010; Sureau et al., 1994) showing that M is dispensable for infectivity of viral particles (Figure 1-figure supplement 3).

Altogether, these results suggested that the determinants of membrane fusion are harbored within L and S GPs.

Next, aiming to identify a fusion peptide in either protein, we used a computational approach to pinpoint regions of the HBV GPs that may potentially interact with membrane bilayers. Using Membrane Protein Explorer (MPEx), a tool based on the Wimley-White Interfacial Hydrophobicity Scale (Snider et al., 2009), five regions of high interfacial hydrophobicity were identified (Figure 2-figure supplement 1A). Two out of the five hydrophobic regions did not correspond to HBV GP transmembrane regions (TM1, TM2, and TM3/TM4), and therefore were considered as candidate fusion peptides (Figure 2A, 2B). The first predicted segment comprised amino acids 48 to 66 that partially overlap with the preS1 domain. The second segment, which includes amino acids 127 to 145, is included in the preS2 region. Our prediction analyzes indicated that the first segment (ΔG=-3.38) was more likely to be a fusion peptide than the second one (ΔG=-0.85) (Figure 2-figure supplement 1B). Considering the Wimley-White scale, a set of mutants was designed to alter the hydrophobicity of the two predicted segments (Figure 2B and Figure 2-figure supplement 1B). In the first segment, three mutants were studied by changing the aromatic residues to an alanine or glutamate: F52A, F56A, W66A, F52A/W66A (FW/AA) and F52E/W66E (FW/EE), or a glycine to an alanine (G53A). In the second segment, four mutants were considered: Y129A, F130A, S136E, L144A; while the first two mutants targeted aromatic residues, S136 and L144 were also considered important because they are at the center of the predicted region and have a relatively high hydrophobicity.

To evaluate the role of these two sequences in HBV fusion, we introduced these single or double mutations in both regions and inserted them in the pT7HB2.7 HBV GP expression plasmid. Each mutant was compared to wt HBV GPs in both infection assays, using HDV particles (Sureau, 2010; Perez-Vargas et al., 2019), and cell-cell fusion assays, as above-described. We found that HDV particles carrying these mutant GPs were produced by Huh7 cells at levels similar to those produced with wt GPs (Figure 2C, 2D), hence ruling out gross misfolding induced by the mutations that would otherwise prevent HBV GPs incorporation on viral particles (Abou-Jaoudé and Sureau, 2007). Interestingly, no infectivity could be detected for most of the mutations introduced in the preS1 peptide (Figure 2E), whereas the HDV particles with mutations in the preS2 peptide showed levels of infectivity that were similar to those obtained with the wt GPs (Figure 2F). Correlating with the results of these infection assays, we found that the mutants in the preS1 peptide that prevented HDV infectivity also abrogated cell-cell fusion activity (Figure 2G) in a manner unrelated to the levels of GPs

cell surface expression (Figure 2I and Figure 2-figure supplement 2). In contrast, mutations in the preS2 peptide displayed the same levels of cell-cell fusion activity as compared to wt (Figure 2H, 2J). Altogether, these results indicated that the preS1 region harbors a potential fusion peptide.

Stabilizing cross-strand disulfide exchanges in HBV S protein prevents membrane fusion. Next, we sought to investigate the mechanisms that could induce fusion-activating conformational changes in the HBV GPs, leading to exposure of the fusion peptide. As neither the HBV receptor interaction nor the acidic pH could trigger membrane fusion (Figure 1), we thought that conformational rearrangement of HBV GPs might involve reshuffling of their disulfide bonds. Indeed, previous studies showed that cysteine residues of the HBV S antigenic loop are essential for HDV infectivity and that viral entry is blocked by inhibitors of thiol/disulfide exchange reactions, such as TCEP, DTT, DTNB or AMS (Abou-Jaoudé and Sureau, 2007). Thus, to extend the notion that thiol/disulfide exchange reactions are implicated during membrane fusion and entry, we performed HBV infection and fusion assays in the presence of DTNB, an alkylator agent. First, using different DTNB concentrations that were added either at the onset of infection or at 16h post-infection, we confirmed that DTNB could block HDV infection in a dose-dependent manner, but only when it was added at the onset of infection (Abou-Jaoudé and Sureau, 2007) (Figure 3-figure supplement 1). Second, using time-of-addition experiments, we found that DTNB could inhibit infection only if added within the first 2 hours after inoculation with HDV particles (Figure 3A). These results suggested that DTNB blocks a thiol/disulfide exchange reaction that could be necessary at an early step of infection, such as a trigger of the fusion mechanism, though not at a later stage of the entry process. Third, to evaluate the effect of DTNB in membrane fusion, we performed cell-cell fusion assays in presence of DTNB, which was added at the onset of cell co-cultures *vs*. at 16h after seeding the cell co-cultures. We showed that DTNB added during the co-culture neither induced cytotoxicity (Figure 1-figure supplement 2) nor affected expression of HBV glycoproteins on the cell surface (Figure 3C, 3D). Yet, we found a dose-dependent reduction of the level of cell-cell fusion when DTNB was added immediately after cell-cell contact, whereas we detected a much lower effect in fusion activity when DTNB was added at 16h after cell contact (Figure 3B).
Altogether, these results suggested a role of the disulfide bonds network during HBV membrane fusion steps, perhaps at the level of the fusion trigger.

To address this possibility and to identify potential mechanisms involved in fusion triggering, we focused on the “a” determinant of protein S that exhibits eight conserved Cys, which, for some of them, are in strong proximity in the sequence (Figure 4A). To avoid trivial contact predictions between consecutive Cys, we defined four Cys-containing regions in a way that Cys pairs that are potentially in contact should have a sequence separation of at least four amino acids. The first Cys-containing

region includes C270, the second C284 and 287, the third C300, C301 and C302, and the last one C310 and C312 (Figure 4A). We applied secondary and tertiary structure prediction methods together with the contact prediction method RaptorX (Ma et al., 2015; Wang et al., 2017), based on coevolution signals, to predict disulfide connectivity in the “a” determinant, which may identify which Cys forms disulfide bonds. Notably, RaptorX predicted structural contacts between either region (Figure 4-figure supplement 1) and we highlighted pairs of residues in contact in the four Cys-regions, with the strongest signal detected between the third and fourth regions (Figure 4B). Next, applying the JPred secondary structure prediction method (Cole et al., 2008), we predicted two β-strands in the Cys-rich regions delimited by the S segments 298-303 and 310-313 (Figure 4A). Then, considering the secondary structure prediction and the contact prediction, we built a three-dimensional model for the region 294-317 (Figure 4C), which indicated that this sequence is compatible with a β-hairpin structural motif containing a cross-strand disulfide (CSD) between C301 and C310. Finally, through the analysis of its five χ dihedral angles (Figure 4-figure supplement 2), this disulfide bond was classified in a “-HStaple conformation”, which is a particular type of disulfide geometry associated with allosteric functions by triggering a conformational change upon switching between the reduced and oxidized states (Chiu and Hogg, 2019; Hogg, 2003).

We therefore hypothesized that the redox state of this disulfide may act as an allosteric switch that could contribute to control conformational rearrangements of the S protein. Thus, we used our structural model of the C301-C310 disulfide bond to design a mutant of S that could disrupt this hypothetical allosteric function, *i.e.*, the T303C/G308C double mutant that induces an additional C303-C308 disulfide bond (Figure 4C). Further molecular dynamics (MD) simulations (1,000 frames per MD trajectory) carried out to differentiate between allosteric and structurally stabilizing disulfides, where the disulfides can be classified based on their angles (Figure 4-figure supplement 2), showed that the T303C/G308C mutant predominantly forms a structural disulfide bond.

Aiming to validate our prediction that an additional disulfide bond between the two β-strands could, by stabilizing the 298-313 β-hairpin motif, prevent membrane fusion from occurring, we produced HDV particles carrying the individual (T303C or G308C) and double (T303C/G308C) mutations in HBV GPs. By measuring HDV RNAs in cell supernatants, we found that all mutants could produce comparable levels of viral particles relative to wt virus (Figure 5A), suggesting absence of gross alterations of HBV GP conformation that would otherwise preclude virion assembly (Abou-Jaoudé and Sureau, 2007). Importantly, we found that while HDV particles generated with GPs harboring the individual mutations were as infectious as wt, those that were produced with the T303C/G308C double mutation (noted TG/CC in Figure 5) and the putative additional C303-C308 CSD bond were not infectious (Figure 5B). Moreover, we found that HDV particles harboring GPs with this T303C/G308C mutation had similar binding levels on Huh7 cells than those generated with wt GPs (Figure 6A), underscoring a post-binding defect. Then, to address this possibility, we performed cell-cell fusion

assays with either HBV GP mutant, which were readily expressed at the cell surface (Figure 5C). We found that whereas the single mutations displayed similar fusion activity as compared to wt HBV GPs, the T303C/G308C double mutation completely prevented HBV GP-induced cell-cell fusion activity (Figure 5D).

Altogether, these results suggested that the putative C303-C308 additional disulfide bond stabilizing the loop containing the C301-C310 CSD bond inhibited HBV entry and fusion, perhaps by preventing conformational rearrangements of HBV GPs that are required for promoting membrane fusion.

ERp57 is a protein disulfide isomerase that promotes HBV entry and infectivity *in vivo*. We reasoned that isomerization of the C301-C310 CSD (Figure 4) or of another CSD of the AGL determinant with allosteric functions could facilitate some conformational rearrangements required to promote membrane fusion. We therefore hypothesized that such an isomerization could be induced by a host factor from the Protein Disulfide Isomerase (PDI) family, which are enzymes that can both reduce and oxidize disulfide bonds.

To address if PDIs are involved in HBV entry, we tested the effect of inhibitors (NTZ, EGCG, Rutin, Bacitracin, PX-12) that target different PDI species (PDIA1, ERp5, ERp57, TMX1) for their effect in cell entry of viral particles. First, through binding assays of viral particles to Huh7 or Huh7-NTCP cells performed in the presence of either inhibitor, we found that none of these inhibitors affected binding of HDV particles generated with either wt or T303C/G308C mutant GPs (Figure 6A). Second, using infection assays with Huh7-NTCP cells pre-incubated with either inhibitor, we found that HDV particles had strongly reduced infectivity in presence of NTZ and EGCG inhibitors that both target ERp57 (Figure 6B). Third, we confirmed these results using infection assays with authentic HBV particles (Figure 6C). Finally, to demonstrate that the inhibitors acted at the level of membrane fusion, we performed cell-cell fusion assays, as above-described, whereby either inhibitor was added at the onset of co-cultures of HBV GP-expressing Huh7 donor and Huh7-NTCP-Tat indicator cells, and was kept throughout the assay period. Remarkably, we found a strong reduction of the levels of cell-cell fusion with the same drugs that inhibited HDV infection (Figure 6D). Hence, these results suggested a potential role of ERp57 in HBV membrane fusion.

Next, aiming to confirm and extend these findings, we selected a subset of the above PDIs, *i.e.*, ERp46, ERp57 and ERp72, that displayed low but significant expression at the surface of Huh7 cells (Figure 7A), in agreement with a previous report (Turano et al., 2002). We down-regulated either PDI in target cells *via* transduction of Huh7-NTCP cells with shRNA-expressing lentiviral vectors (Figure 7-figure supplement 1 and Figure 7-figure supplement 2). We found that down-regulation of ERp57, though not ERp46 or ERp72, strongly reduced the levels of HDV (Figure 7B) and HBV infection (Figure 7C) and of cell-cell fusion (Figure 7D). Finally, through confocal microscopy analysis of Huh7-

NTCP cells (Figure 8A), we investigated the co-localization between ERp57 and Rab5 (early endosomes), Rab7 (late endosomes), Rab11 (recycling endosomes) or Lamp1 (lysosomes). The quantifications of these results showed that ERp57 could be detected in late endosomes but poorly in the other above-tested locations (Figure 8B), in line with the notion that fusion of HBV particles occurs in late endosomes (Macovei et al., 2013). Thus, ERp57 can be found at locations compatible for both cell-cell fusion and cell-free entry by internalization.

Altogether, these results indicated that ERp57 is likely a protein disulfide isomerase that promotes HBV entry at a membrane fusion step.

Finally, we sought to demonstrate that ERp57 inhibition may prevent HBV propagation *in vivo* using NTZ, which has a short half-life of about 1.5h (Ruiz-Olmedo et al., 2017; Stockis et al., 1996). We generated a cohort of liver humanized mice (HuHep-mice) derived from the NFRG mouse model (Azuma et al., 2007) (Figure 9A). We retained the animals that displayed >15 mg/mL of human serum albumin (HSA), which corresponds to 40-70% of human hepatocytes in the liver (Calattini et al., 2015). In agreement with previous reports (Perez-Vargas et al., 2019), these animals supported HBV infection (Group#1) for several weeks/months (Figure 9B; see Figure 9-figure supplement 1 for individual mice). The second group of HuHep mice was treated with NTZ 30min prior to inoculation with HBV, and then, treated again with NTZ 1h later. We found that viremia in this group was delayed by about 4 weeks, as compared to Group#1 for which HBV could disseminate immediately after inoculation. This indicated that the blocking of ERp57 could prevent HBV infection *in vivo*.

Discussion

The entry process of enveloped viruses into cells is the series of all events that take place from the attachment of the virus to the host cell until the release of its genome in the cytoplasm. It is a finely regulated and complex process with several steps, in which many viral and cellular factors are involved. The first interaction often occurs with HSPGs. It may lack specificity but serves to give a virus an initial catch hold from which it can recruit specific receptors and entry co-factors that drive the reactions leading to entry. Fusion is the last step of enveloped virus entry and allows the release of the viral capsid in the cytoplasm following the merging of the viral membrane with a membrane of the infected cell. The interactions with the target cell that trigger conformational changes of the viral surface glycoproteins, ultimately leading to the insertion of their fusion peptide into the cell membrane, vary widely for enveloped viruses and can be divided into different scenarios. In a first one (*e.g.*, HIV), fusion is triggered directly by the interaction of the viral glycoprotein with its cellular receptor, through allosteric conformational rearrangements. In some cases, a sequential interaction with additional host

factors is required to trigger the conformational changes required for fusion. In a second scenario (*e.g.*, influenza virus), the interactions with the receptor at the cell surface leads to the endocytosis of viral particles, which is followed by GP protonation in the low pH environment of the intracellular endosomal organelles that triggers the fusogenic conformational change. In a third scenario (*e.g.*, Ebola virus), the initial interactions of the virion with the cell surface trigger its endocytosis followed by a second interaction with an internal receptor, often found in late endosomes, which is preceded by proteolytic cleavage of the fusion protein by an endosomal protease, leading to fusion activation (Harrison, 2015; White and Whittaker, 2016). Finally, for certain viruses (*e.g.*, Sindbis virus), the fusion protein requires an activating redox reaction involving disulfide bonds of their glycoproteins to induce membrane fusion (Key et al., 2015; Rey and Lok, 2018).

Using a cell-cell fusion assay, we found that HBV fusion activity reached similar levels whether indicator cells expressed or not HSPG and/or NTCP but was not increased when the cell co-cultures were exposed at low pH, in contrast to *bona fide* pH-dependent GPs such as VSV-G or CCHFV Gn/Gc (Figure 1). That both HSPG and NTCP, which are respectively HBV virion membrane capture molecules (Leistner et al., 2008; Schulze et al., 2007) and specific entry factors (Ni et al., 2014; Yan et al., 2015), are not required for cell-cell fusion highlights that this fusion assay reveals late entry events, such as those occurring after virus interaction with either factor. Similarly, for other viruses such as *e.g.*, influenza virus or hepatitis C virus (HCV), binding to their cell entry receptor is not a requirement in both cell-cell fusion (Lin and Cannon, 2002) and liposome fusion (Lavillette et al., 2006) assays triggered by low pH treatment. Thus, while it is clear that cell-cell fusion does not recapitulate *per se* all the events required to promote cell entry of viral particles since it bypasses the step of internalization that subsequently allows membrane fusion in endosomes that are required for entry of the above-mentioned viruses and of HBV (Macovei et al., 2013; Iwamoto et al., 2019), it a suitable experimental tool for investigating some of the structural and functional determinants that promote envelope glycoprotein membrane-fusion activity (Earp et al., 2004). Accordingly, our results indicate that the trigger for the HBV membrane fusion mechanism not only is independent of an allosteric interaction of its GPs with the NTCP receptor but also is independent of GPs protonation that is induced by the low pH environment of endosomes. That low pH does not increase HBV cell-cell fusion agrees with previous results indicating that pharmacological agents that raise or neutralize the pH of the endocytic pathway had no effect on HBV infection (Macovei et al., 2010, 2013; Rigg and Schaller, 1992).

Previous results from the group of Camille Sureau showed that cysteine residues of the HBV antigenic loop are essential for HDV infectivity and that viral entry is blocked by inhibitors of thiol/disulfide exchange reaction (Abou-Jaoudé and Sureau, 2007). Our results extend this notion as they indicate that such reactions seem to be necessary to mediate a critical early post-binding event but not at a

later stage of the infection process since no effect in virus infectivity could be detected when DTNB was added at 4h post-infection (Figure 3). Since isomerization of disulfide bonds has been shown to be crucial for conformational rearrangements of GPs from other enveloped viruses leading to fusion (Fenouillet et al., 2007), we sought to investigate if and how such reactions could be implicated during the membrane fusion step of HBV entry. Here, using our cell-cell fusion assay, we found that DTNB blocked HBV GP-mediated membrane fusion (Figure 3B). Altogether, these results indicated a role of disulfide bond network of S GP during HBV membrane fusion.

Capitalizing on the above-mentioned experimental information that inhibitors of thiol/disulfide exchange reactions alter virus entry, we sought to examine how disulfide bonds of the HBV GPs, or rather, how a potential reshuffling of its disulfide bonds profile, could be important for HBV entry. Indeed, cross-strand disulfides occurring in some viral surface GPs are believed to play a role in virus entry (Barbouche et al., 2003; Jain et al., 2007; Rosenthal et al., 1998; Wouters et al., 2004). Particularly, allosteric disulfide bonds can modulate the activity of the proteins in which they reside by mediating a structural change when they are reduced or oxidized (Hogg, 2003; Schmidt et al., 2006). Allosteric control of protein function is defined as a change in one site (the allosteric site) that influences another site by exploiting the protein's flexibility; an allosteric disulfide bond represents the "allosteric site" and the conformational change triggered by cleavage of such bonds alters protein function. For the HBV S protein, we used the contact prediction method RaptorX (Ma et al., 2015, Wang et al., 2017) to predict contacts between four Cys-rich regions of the AGL determinant (Figure 4), which highlighted that two of these regions may likely interact: *i.e.*, the Cys-rich regions III and IV (Figure 4-figure supplement 1). Using the secondary structure prediction method JPred (Cole et al., 2008), we proposed that these regions organize in two β-strands and we constructed a three-dimensional model of the region 294-317 of the HBV S GP, which indicated that this sequence is compatible with a β-hairpin structural motif containing a CSD bond between C301 and C310 (Figure 4). Interestingly, the analysis of the signs of the five χ dihedral angles defined by the Cys residues allowed to classify this particular disulfide bond in a -HStaple conformation, which is a particular type of disulfide geometry associated with allosteric functions that is known to trigger conformational changes upon switching between the reduced and oxidized states (Chiu and Hogg, 2019; Schmidt et al., 2006). Hence, we hypothesized that the redox state of the C301-C310 disulfide bond may act as an allosteric switch controlling conformational rearrangements of the HBV GP leading, ultimately, to exposure of the fusion peptide. Of note, the β-hairpin region with the predicted CSD lies at the surface of the S protein according to a three-dimensional *in silico* model (van Hemert et al., 2008), which may allow interactions with other HBs subunits and/or cellular factors. Yet, to test our structural and dynamic model involving a C301-C310 CSD bond in S GP (Figure 4), we reasoned that creating an additional, neighboring disulfide bond between positions 303 and 308 may stabilize the β-hairpin motif

(Figure 4), which may prevent molecular rearrangements and thus, membrane fusion to occur. The *in silico* analysis indicates that the T303C/G308C double mutant most probably generates two structural CSD according to our JPred-based (Cole et al., 2008) structural modelling, which affects the structural conformation of the C301-C310 CSD that is no longer classified as an allosteric bond. When we tested the T303C/G308C mutation in functional assays, we found that the mutant HBV GPs induced an almost complete loss of infection and fusion activity (Figure 5), hence suggesting that by stabilizing cross-strand disulfide exchange, the putative additional disulfide bond prevented conformational rearrangements of HBV GPs that are required for promoting membrane fusion. One possibility is that such stabilization could prevent an isomerization of the C301-C310 CSD bond that generates alternative disulfide bond(s) such as, for example, between C284 and C310 that was proposed in a previous study (Mangold et al., 1995). Yet, the antigenic loss of S induced by these mutations did not allow us to design an assay that would detect the additional disulfide bond in the T303C-G308C mutant nor the block of conformational rearrangements that is suggested by its phenotype.

Assuming that the isomerization of the C301-C310 allosteric CSD or of other thiols/disulfides of the AGL determinant could facilitate the conformational rearrangements of HBs required to promote HBV membrane fusion, we hypothesized that such isomerization could be induced by a host factor from the PDI family, which are enzymes that can both reduce and oxidize disulfide bonds. Protein disulfide isomerases consist of a family of 21 structurally related proteins with a thioredoxin-like domain. Most of these isomerases have a CXXC motif that catalyzes formation, reduction and rearrangement of the disulfide bonds in proteins (Abell and Brown, 1993). These isomerases are primarily involved in the folding of proteins in the ER, catalyzing formation of their disulfide bonds, and most of these isomerases have ER retention signals. However, some isomerases from the PDI family have also been shown to be present at the cell surface, both in functional and in biochemical assays (Turano et al., 2002). Accordingly, cell surface-localized PDIs are involved in processes such as cell adhesion, nitric oxide signaling, and in cell entry of different viruses (Diwaker et al., 2013; Fenouillet et al., 2007). In support of the notion that PDIs are involved in HBV entry, we found that inhibitors that target different PDI members could block infection and cell-cell fusion though not the binding of viral particles to the cell surface. Of note, we found that bacitracin, which targets PDIA1, did not inhibit HBV entry and membrane fusion, in line with a previous study showing that it could not inhibit HDV entry (Abou-Jaoudé and Sureau, 2007). While the above ruled out PDIA1 as an entry co-factor of HBV, we found a strong reduction of the levels of HBV and HDV infection as well as of HBV-induced cell-cell fusion when we used the NTZ and EGCG inhibitors (Figure 6), which target ERp57 (Müller et al., 2008; Pacello et al., 2016). Consistently, we detected a low but significant expression of ERp57 as well as of ERp46 and ERp72 at the cell surface (Figure 7), in agreement with a previous study (Turano et al., 2002). Furthermore, we detected ERp57 in late endosomes (Figure 8), which is meaningful since

previous reports showed that HBV infection of HepaRG cells depends on Rab5 and Rab7 (Macovei et al., 2013), which are GTPases involved in the biogenesis of endosomes, and that the epidermal growth factor receptor is a host-entry cofactor that interacts with NTCP and mediates HBV internalization (Iwamoto et al., 2019). Using a gene silencing approach, we confirmed that down-regulation of ERp57 but not of these alternative PDIs could decrease the levels of HDV and HBV infection as well as of cell-cell fusion (Figure 7). Importantly, we showed that a short time treatment of liver humanized mice with NTZ could delay HBV infection by *ca*. 2-4 weeks (Figure 9). Since NTZ has a short half-life of about 1.5h *in vivo* (Ruiz-Olmedo et al., 2017; Stockis et al., 1996) and since NTZ was administrated at very short times before and after HBV inoculation, we calculated that less than 10% of the drug was still present in those mice at 7h post-infection, which likely precludes an effect on HBV post-entry steps (Korba et al., 2008). Altogether, these results support the role of ERp57 at early steps of HBV infection and validate this PDI as a therapeutic target. Note that our results did not discard the possibility that some other PDIs could also play a role during HBV entry into cells.

The fusion-mediating GPs of enveloped viruses contain a sequence, termed fusion peptide that interacts with and destabilizes the cellular target membrane. Such an event is finely controlled so as to occur at the appropriate time and location and to prevent fortuitous inactivation of GP fusion activity and virus infectivity. Hence, a conformational change in these GPs is a requirement to induce the accessibility and function of the fusion peptide segment. Candidate fusion peptides are generally identified as hydrophobic sequences, of *ca*. 16 to 26 residues in length, that are conserved within a virus family and that may adopt α-helical conformation with strongly hydrophobic faces. They can be internal or located at the amino-terminus of fusion GP subunits (Apellániz et al., 2014; Epand, 2003; Martin et al., 1999). There are a number of criteria that characterize fusion peptide segments and, while none of these criteria taken individually are absolute to define a fusion peptide segment, they are sufficiently restrictive to predict if a given region of a protein presents features of a fusion peptide segment (Delos and White, 2000; Delos et al., 2000), which needs to be further functionally tested.
Previously, a conserved peptide comprising 23 amino acids at the N-terminal end of the HBV S protein and overlapping its TM1 sequence was shown to interact with model membranes, causing liposome destabilization in a pH-dependent manner (Berting et al., 2000; Rodríguez-Crespo et al., 1994, 1995, 1999). However, it was also demonstrated that hydrophobic residues in TM1 were critical for S protein expression as well as for infectivity (Siegler and Bruss, 2013). An essential role of TM1 in fusion mechanism, albeit in a pH-independent manner, could be shown for the duck hepatitis B virus (DHBV) (Chojnacki et al., 2005; Grgacic and Schaller, 2000), although there is also evidence for the involvement of the preS domain of DHBV at an early step of infection, likely during the fusion process (Delgado et al., 2012).

Here, through a computational hydropathy analysis of the HBV GPs, we identified two potential short sequences within the preS1 and preS2 regions that may potentially interact with membrane bilayers. To validate these predictions, we characterized in both infection and cell-cell fusion assays HBV GP mutants in key positions in either sequence. We found that while none of the mutations in the preS2 segment altered infection or membrane fusion activities, mutations in the preS1 sequence induced an almost complete loss of infectivity and cell-cell fusion (Figure 2). Note that these mutants had similar if not identical levels of cell surface expressed L, M and S proteins and/or capacity to induce the formation of HDV particles. These results suggested that the preS1 region harbors a fusion peptide in addition to the NTCP binding determinant.

Overall, our study characterizes some crucial determinants of HBV entry and membrane fusion. The mechanism by which fusion proteins are activated and undergo conformational rearrangements or fusion intermediates is a particularly complex process involving several regions of viral surface GPs. Our results suggest that for HBV, this mechanism could be triggered by ERp57, allowing a thiol/disulfide exchange reaction to occur and regulate isomerization of critical CSD(s), which ultimately results in the exposition of the fusion peptide that seems to be located within the preS1 region.

Material and Methods

Key Resources Table

Reagent type (species) or resource	Designation	Source or reference	Identifiers	Additional information
strain, strain background (*M. musculus,* females and males)	NOD-FRG mice	DOI: 10.1038/nbt1326 DOI : 10.1074/jbc.M115.662999		Breeding and experimentation in PBES – Originally purchased to YEcuris corporation
strain, strain background (HBV)	Hepatitis B virus (HBV)	This paper		HBV, genotype D, produced by co-transfection of HepG2.2.15 cells with plasmids pCiHB(env-) and pT7HB2.7

strain, strain background (HDV)	Hepatitis D virus (HDV)	This paper		HDV, genotype 1, produced by co-transfection of Huh7 cells with plasmids pSVLD3 and pT7HB2.7, or variant constructs
cell line (*Homo-sapiens*)	Huh7 - hepatocarcino ma cells	PMID: 6286115		
cell line (*Homo-sapiens*)	Huh7-NTCP	This paper		Generated by transduction with pLX304NTCP retroviral vector and selection with blasticidin
cell line (*Homo-sapiens*)	Huh7-Tat (H-tat) cells	This paper		Generated by transduction with LXSN-tat retroviral vector and selection with G418
cell line (*Homo-sapiens*)	H-tat cells down regulated for ERp46, ERp57 or ERp72	This paper		Generated by transduction of H-tat cells with shRNA lentiviral vectors against ERp46, ERp57 or ERp72 followed by selection with puromycin
cell line (*Homo-sapiens*)	Huh7-NTCP-Tat (N-tat) cells	This paper		Generated by transduction of Huh7-NTCP cells with LXSN-tat retroviral vector
cell line (*Homo-sapiens*)	N-tat cells down regulated for ERp46, ERp57 or ERp72	This paper		Generated by transduction of N-tat cells with shRNA lentiviral vectors against ERp46, ERp57 or ERp72 followed by selection with puromycin
cell line (*Homo-sapiens*)	HepG2.2.15 human hepatoma cells	From David Durantel lab		Production of HBV particles

cell line (*Homo-sapiens*)	293T human kidney cells	ATCC	CRL-1573	Production of retro- and lentiviral particles
cell line (Cricetulus griseus, female)	CHO-K1 Chinese hamster ovary cells	ATCC	CCL-61	Cell-cell fusion assays
transfected construct (human)	pLX304NTCP	DNASU plasmid repository	HQ447437	retroviral construct to transfect and express NTCP
transfected construct (HBV)	pSVLD3	DOI: 10.1128/JVI.63.5.1945-1950.1989		Harbors a trimer of the HDV, genotype 1 genome. Used for production of HDV particles
transfected construct (HBV)	pT7HB2.7	DOI: 10.1128/JVI.68.6.4063-4066.1994		Gift from Camille Sureau, used for production of HBV and HDV particles and expression of HBV envelope proteins
transfected construct (HBV)	pT7HB2.7Mless (noM)	This paper		Generated for expression of HBV L and S proteins (M protein is silenced)
transfected construct (HBV)	pCiL	doi: 10.1128/JVI.77.9.5519-5523.2003		Encodes only the L-HBsAg protein
transfected construct (HBV)	pCIS	doi: 10.1128/JVI.80.10.4648-4655.2006		Encodes only the S-HBsAg protein
transfected construct (CCHFV)	pCAGGS_GP/wt-M	DOI: 10.1128/JVI.03691-14		Major open reading frame of CCHFV M-segment subcloned into pCAGGS
transfected construct (HBV)	pCIHB(env-)	DOI: 10.1128/JVI.00621-06		Gift from Camille Sureau, used for production of HBV particles
transfected construct (HIV1-Tat)	LXSN-tat retroviral vector	DOI: 10.1128/JVI.73.3.1956-1963.1999		HIV-1 *tat* gene cloned into the LXSN retroviral vector

transfected construct (HIV1-LTR)	pLTR-luc	DOI: 10.1016/0378-1119(90)90032-m		gift from Olivier Schwartz, contains a 722-base pair *Xho*I (−644)-*Hin*dIII (+78) fragment from HIV-1 placed in front of the luciferase reporter gene
transfected construct (VSV)	phCMV-VSV-G	DOI: 10.1016/s0091-679x(08)60600-7		To express the envelope protein of VSV
transfected construct (human)	shRNA against ERp46 (ERp46-shRNA 1)	Sigma	NM_022085 / TRCN0000064353 / PLKO.1	Lentiviral construct to transfect and express the shRNA.
transfected construct (human)	shRNA against ERp46 (ERp46-shRNA 2)	Sigma	NM_022085 / TRCN0000064354 / PLKO.1	Lentiviral construct to transfect and express the shRNA.
transfected construct (human)	shRNA against ERp57 (ERp57-shRNA 3)	Sigma	NM_005313 / TRCN0000319038 / PLKO	Lentiviral construct to transfect and express the shRNA
transfected construct (human)	shRNA against ERp57 (ERp57-shRNA 4)	Sigma	NM_005313 / TRCN0000147738 / PLKO.1	Lentiviral construct to transfect and express the shRNA
transfected construct (human)	shRNA against ERp72 (ERp72-shRNA 3)	Sigma	NM_004911 / TRCN0000289676 / PLKO.1	Lentiviral construct to transfect and express the shRNA
transfected construct (human)	shRNA against ERp72 (ERp72-shRNA 4)	Sigma	NM_004911 / TRCN0000049334 / PLKO.1	Lentiviral construct to transfect and express the shRNA

transfected construct (human)	shRNA against ERp72 (ERp72-shRNA 5)	Sigma	NM_004911 / TRCN0000307107 / PLKO.1	Lentiviral construct to transfect and express the shRNA
biological sample (*M. musculus*)	Blood samples	PBES (Plateau de Biologie Experimentale de la Souris) SFR Biosciences Lyon		isolated from NOD-FRG mice
antibody	anti-HBsAg antibody, HPR conjugated (goat polyclonal)	DiaSorin	9F80-01	WB(1:400)
antibody	anti-human calnexin (rabbit polyclonal)	Enzo	ADI-SPA-865-F	WB(1:1000)
antibody	anti-mouse TXNDC5/ERp46 (rabbit polyclonal)	Abcam	Ab10292	FACS(1:20) WB(1:1000)
antibody	anti-human ERp57 (mouse monoclonal)	Abcam	Ab13506	FACS(2 µg/10^6 cells) WB(1:10000) IF(1:100)
antibody	anti-human ERp72 (rabbit polyclonal)	Abcam	Ab155800	FACS(1:100) WB(1:1000)
antibody	anti-human NTCP/SLC10A1 antibody, PE conjugated (rabbit polyclonal)	Bioss Antibodies	bs-1958R-PE	FACS(1:100)
antibody	anti-human Rab5 (rabbit monoclonal)	Cell Signaling Technology	(C8B1):3547	IF(1:200)

antibody	anti-human Rab7 (rabbit monoclonal)	Cell Signaling Technology	(D95F2):9367	IF(1:100)
antibody	anti-human Rab11 (rabbit monoclonal)	Cell Signaling Technology	(D4F5):5589	IF(1:50)
antibody	anti-human Lamp1 (rabbit monoclonal)	Cell Signaling Technology	(D2D11):9091	IF(1:200)
sequence-based reagent	F52A	This paper	preS1 mutagenesis PCR primers	GTAGGAGCTGGAGCAG CCGGGCTGGGTTTCAC
sequence-based reagent	F52E	This paper	preS1 mutagenesis PCR primers	GTAGGAGCTGGAGCAGA AGGGCTGGGTTTCAC
sequence-based reagent	G53A	This paper	preS1 mutagenesis PCR primers	CTGGAGCATTCGCGCT GGGTTTCAC
sequence-based reagent	F56A	This paper	preS1 mutagenesis PCR primers	TTCGGGCTGGGTGCC ACCCCACCGCA
sequence-based reagent	W66A	This paper	preS1 mutagenesis PCR primers	GAGGCCTTTTGGGGGCG AGCCCTCAGGCTC
sequence-based reagent	W66E	This paper	preS1 mutagenesis PCR primers	GAGGCCTTTTGGGGGAG AGCCCTCAGGCTC
sequence-based reagent	Y129A	This paper	preS2 mutagenesis primers	GAGTGAGAGGCCTGGCTT TCCCTGCTGGTG

sequence-based reagent	F130A	This paper	preS2 mutagenesis primers	GAGAGGCCTGTATGCCCC TGCTGGTGG
sequence-based reagent	S136E	This paper	preS2 mutagenesis primers	CCCTGCTGGTGGCTCCGAA TCAGGAACAGTAAAC
sequence-based reagent	L144A	This paper	preS2 mutagenesis primers	CAGTAAACCCTGTTGCGACT ACTGCCTCTCC
sequence-based reagent	T303C	This paper	CSD mutagenesis primers	CCTCCTGTTGCTGTTGCAAA CCTTCGGACG
sequence-based reagent	G308C	This paper	CSD mutagenesis primers	GTACCAAACCTTCGGACTGT AATTGCACCTGTATTCCC
sequence-based reagent	TG/CC	This paper	CSD mutagenesis primers	GTTGCAAACCTTCGGACTGT AATTGCACCTGTATTCCC
commercial assay or kit	FuGENE HD Trasnfection Reagent	Promega	E2312	Transfection reagent
commercial assay or kit	Dual-Luciferase® Reporter Assay System	Promega	E1910	Quantification of luciferase activity
commercial assay or kit	iScript cDNA synthesis kit	Bio-Rad	1708891	cDNA synthesis
commercial assay or kit	FastStart Universal SYBR Green Master	Roche Sigma	4913850001	Real time qPCR assays
commercial assay or kit	CytoTox-ONE™ Homogen Membrn Integrity Assay	Promega	G7891	Cytotoxicity assay

chemical compound, drug	Bacitracin	Sigma	B0125-250KU	water
chemical compound, drug	NTZ (Nitazoxanide)	Sigma	N0290-50MG	DMSO
chemical compound, drug	EGCG (−)-Epigallocatechin gallate	Sigma	E4268-100MG	water
chemical compound, drug	RUTIN HYDRATE	Sigma	R5143-50G	DMSO
chemical compound, drug	PX-12	Sigma	M5324-5MG	DMSO
chemical compound, drug	DTNB 5,5′-Dithiobis(2-nitrobenzoic acid)	Sigma	D218200-1G	DMSO
chemical compound, drug	EZ-Link Sulfo-NHS-LC-LC-Biotin	Life technologies	21338	
software, algorithm	ImaJ software	ImaJ	RRID:SCR_003070	
software, algorithm	Membrane Protein eXplorer	http://blanco.biomol.uci.edu/mpex/	RRID:SCR_014077	
software, algorithm	RaptorX	http://raptorx.uchicago.edu/	RRID:SCR_018118	
software, algorithm	Jpred	http://www.compbio.dundee.ac.uk/jpred/	RRID:SCR_016504	

software, algorithm	MODELLER	http://salilab.org/modeller/modeller.html	RRID:SCR_008395	
software, algorithm	Clustal X	http://www.clustal.org/clustal2/	RRID:SCR_017055	
software, algorithm	Molecular Modelling Toolkit	http://dirac.cnrs-orleans.fr/MMTK.html		
software, algorithm	GROMACS	http://www.gromacs.org	RRID:SCR_014565	
software, algorithm	UCSF Chimera	http://plato.cgl.ucsf.edu/chimera/	RRID:SCR_004097	
other	Hoechst 33342 stain	Thermo Fisher	H3570	10 µg/ml
other	STREPTAVIDIN AGAROSE RESIN	Thermo fisher	20353	
other	TRI-Reagent	Molecular Research Center Euromedex	TR118-200	RNA extraction

Plasmids. Plasmid pSVLD3 harboring a trimer of the HDV gt1 genome (accession number M21012.1), pCiL encoding the L protein, pCiS encoding the S protein (Komla-Soukha and Sureau, 2006) and pT7HB2.7 encoding the three HBV envelope proteins were a gift from Camille Sureau (Sureau, 2010; Sureau et al., 1994). To induce the expression of L and S only, the pT7HB2.7 plasmid was modified at the M start codon and Kozak consensus sequence in order to silence the expression of M protein, resulting in pT7HB2.7Mless construct. The pCiM plasmid encoding the M protein was constructed by deleting the preS1 region from pCiL until the N-terminal methionine of preS2. All mutations in pT7HB2.7 plasmid were introduced by point directed mutagenesis. The phCMV-VSV-G encoding the G protein from vesicular stomatitis virus (VSV) and pCAGGS-GP/wt-M encoding the Gn and Gc glycoproteins from Crimean-Congo hemorrhagic fever virus (CCHFV) were described previously (Freitas et al., 2020). The plasmid encoding the luciferase reporter under control of an HIV-1 long terminal repeat internal promoter (pLTR-luc) was a gift from Olivier Schwartz and was used as

described before (Lavillette et al., 2007). Mission shRNAs plasmids (Sigma), shRNAs sequences and oligonucleotides used for introducing mutations in HBV GPs are described in Supplementary file 1.

Cells. Huh7 human hepatocarcinoma cells and Huh7-NTCP cells, which were generated by transduction of Huh7 cells with a retroviral vector transducing the NTCP plasmid (pLX304NTCP, DNASU) and selected for blasticidin resistance, were grown in William's E medium (WME) (Gibco, France) supplemented with non-essential amino acids, 2 mM L-Glutamine, 10 mM HEPES buffer, 100 U/mL of penicillin, 100 µg/mL of streptomycin and 10% fetal bovine serum. 293T human kidney cells (ATCC CRL-1573), CHO-K1 (CHO) Chinese hamster ovary cells (ATCC CCL-61) and CHO-pgsB-618 cells (ATCC CRL-2241), which do not produce glycosaminoglycans, were grown in Dulbecco's modified minimal essential medium (DMEM, Gibco) supplemented with 100 U/mL of penicillin, 100 µg/mL of streptomycin, and 10% fetal calf serum. Huh7-Tat and Huh7-NTCP-Tat indicator cells expressing HIV Tat were generated by transduction of Huh7 and Huh7-NTCP cells, respectively, with the LXSN-tat retroviral vector and selected for G418 resistance. HepG2.2.15 human hepatoma cells were used to produce HBV virus, there were maintained in WME medium complemented with 10% fetal bovine serum. Authentication of purchased cell lines was performed by ATCC. Authentication of Huh7 cells was based on expression of human transferrin and serum albumin. Authentication of HepG2.2.15 cells was based on titration of released infectious HBV particles. All cell lines were certified mycoplasma-free, as per our monthly contamination testing.

PDI inhibitors. 5,5-Dithiobis(2-nitrobenzoic acid) (DTNB), Nitazoxanide (NTZ), (−)-Epigallocatechin 3-gallate (EGCG), Rutin, Bacitracin and PX-12 were purchased from Sigma-Aldrich and dissolved in DMSO, ethanol or water according to the manufacturer's instructions.

Antibodies. For western-blot analysis, HBs antigen and calnexin were detected with goat anti-HBV polyclonal antibody (murex, DiaSorin) coupled to horseradish peroxidase (HRP) and rabbit calnexin polyclonal antibody (Enzo), respectively. The rabbit anti-ERp46 (Abcam), mouse anti-ERp57 (Abcam), and mouse anti-ERp72 (Santa Cruz Biotechnology) antibodies were used for detecting protein disulfide isomerase proteins by flow cytometry and western blot. NTCP was detected with polyclonal NTCP/SLC10A1 antibody (Bioss Antibodies) coupled to PE for flow cytometry. Mouse anti-ERp57 (Abcam), Rabbit anti-Rab5, anti-Rab7, anti-Rab11 and anti-Lamp1 (Cell Signaling Technology), and Donkey anti-Rabbit-Alexa-Fluor-488 and Donkey anti-Mouse-Alexa-Fluor-568 (Thermo Fisher) antibodies were used for immuno-fluorescence studies.

shRNA-expressing stable cell lines. 293T cells were seeded 24h prior to transfection with VSV-G plasmid, psPAX2 packaging plasmid, and pLKO.1 expression vector carrying shRNA against ERp46, ERp57, or ERp72 using calcium phosphate precipitation. Medium was replaced 16h post-transfection. Vector supernatants were harvested 24h later, filtered through a 0.45 µm filter. Stable knockdown of ERp72, ERp57 or ERp46 in Huh7-NTCP, Huh7-tat, and Huh7-NTCP-tat cells was performed by selection with puromycin after lentiviral transduction. The knockdown was validated by flow cytometry and western blot using antibodies against ERp46, ERp57 or ERp72.

Cell-cell fusion assays. Huh7 "donor" cells ($2.5x10^5$ cells/well seeded in six-well tissue culture dishes 24 h prior to transfection) were co-transfected using FuGENE 6 transfection reagent (Promega) with 3 µg of pT7HB2.7- wt or mutated glycoproteins and 50 ng of pLTR-luc reporter plasmid. For a positive control, cells were co-transfected with 3 µg of either pCAGGS-GP/wt-M, expressing CCHFV GPs, or 1 µg of phCMV-VSV-G and with 50 ng of the pLTR-luc plasmid. For negative controls, cells were co-transfected with 2 µg of an empty phCMV plasmid and 50 ng of the pLTR-luc plasmid. Twelve hours later, transfected cells were detached with Versene (0.53 mM EDTA; Gibco), counted, and reseeded at the same concentration (10^5 cells/well) in twelve-well plates. Huh7-Tat or Huh7-NTCP-Tat indicator cells, detached with EDTA and washed, were then added to the transfected cells ($3x10^5$ cells per well). After 24h of cocultivation, the cells were washed with PBS, incubated for 3 min in fusion buffer (130 mM NaCl, 15 mM sodium citrate, 10 mM MES [2-(N-morpholino)ethanesulfonic acid], 5 mM HEPES) at pH4, pH5 or pH7, and then washed three times with normal medium. The luciferase activity was measured 24h later using a luciferase assay kit according to the manufacturer's instructions (Promega).

HDV particles production and infection. Huh7 cells were seeded in 10 cm plates at a density of 10^6 cells per plate and were transfected with a mixture of 2.5 µg of pSVLD3 plasmid and 10 µg of plasmid allowing the expression of surface envelope glycoproteins of VSV or HBV using FuGENE 6 transfection reagent (Promega), as described previously (Perez-Vargas et al., 2019). Transfected cells were grown for up to 9 days in primary hepatocyte maintenance medium containing 2% DMSO to slow cell growth.

The supernatants of virus producer cells were filtrated through 0.45 nm-pore filters and were analyzed by RTqPCR for detection of HDV RNA, using the primers described below. These supernatants were also used for infection experiments in Huh7-NTCP cells or PDI-down-regulated Huh7-NTCP cells, which were seeded in 48-well plates at a density of $1.5x10^4$ cells per well. Infected cells were cultured in primary hepatocyte maintenance medium containing 2% DMSO following infection. RTqPCR assays were used to assess infectivity of viral particles at 7 days post-infection.

For inhibition assays, drugs were incubated with cells for 2h at 37°C before virus addition or at different times post-infection and the infectivity was assessed 7 days post-infection by RT-qPCR.

Binding assays. HDV wt particles (10^7 GE) were added to Huh7-NTCP cells and incubated for 1h at 4°C. Unbound virions were removed by three washes with cold PBS, and RTqPCR was used to assess the amount of bound viral particles.

RTqPCR detection of HDV RNAs in virus-producer and in infected cells. Cells were washed with phosphate-buffer saline (PBS) and total RNA was extracted with TRI Reagent according to the manufacturer's instructions (Molecular Research Center). RNAs were reverse transcribed using random oligonucleotides primers with iScript (Bio-Rad). The following specific primers were used: for HDV RNA quantification, forward primer 5'-GGACCCCTTCAGCGAACA and reverse primer 5'-CCTAGCATCTCCTCCTATCGCTAT. qPCR was performed using FastStart Universal SYBR Green Master (Roche) on a StepOne Real-Time PCR System (Applied Biosystems). As an internal control of extraction, *in vitro*-transcribed exogenous RNAs from the linearized Triplescript plasmid pTRI-Xef (Invitrogen) were added to the samples prior to RNA extraction and quantified with specific primers (5′-CGACGTTGTCACCGGGCACG and 5′-ACCAGGCATGGTGGTTACCTTTGC). All values of intracellular HDV RNAs were normalized to GAPDH gene transcription. For GAPDH mRNAs quantification, we used the forward 5'-AGGTGAAGGTCGGAGTCAACG and reverse 5'-TGGAAGATGGTGATGGGATTTC primers.

Western-blot analyses. The proteins from pelleted cell supernatants or extracted from total cell lysates were denatured in Lammeli buffer at 95°C for 5 min and were separated by sodium dodecyl sulfate polyacrylamide gel electrophoresis and then transferred to nitrocellulose membranes (GE Healthcare). Membranes were blocked with 5% nonfat dried milk in PBS and incubated at 4°C with a rabbit or mouse antibody diluted in PBS-0.01% milk, followed by incubation with a IRdye secondary antibody (Li-Cor Biosciences). Membranes visualization was performed using an Odyssey infrared imaging system CLx (LI-COR Biosciences).

For cell surface biotinylation, Huh7 cells were transfected into 10 cm plates with plasmid encoding wt or mutant HBV GPs. After 48h, the cell monolayers were rinsed three times with ice-cold PBS and overlaid with 0.5 ml biotin solution (0.5 mg sulpho-N-hydroxysuccinimide–biotin (Pierce) per ml of PBS, pH 7.2). The cells were then labeled for 30 min at 4°C. The biotin solution was removed and the cells were rinsed once with ice-cold 100 mM glycine solution and then incubated for 15 min with 100 mM glycine at 4 °C to stop the reaction. The last washing step was performed with ice-cold PBS. Proteins were solubilized by the addition of 1 ml RIPA buffer and equivalent quantities of protein lysates from each sample (Nanodrop quantification, Thermofisher) were immunoprecipitated with

Biotin-agarose beads. Proteins were electrophoresed under reducing conditions in SDS–PAGE followed by electrophoretic transfer to nitrocellulose. Surface-biotinylated proteins were detected with anti-HBV antibody (murex) coupled to horseradish peroxidase (HRP) and enhanced chemiluminescence (ECL; Roche). The membranes of biotinylated samples were routinely re-probed with anti-calnexin antibody to confirm the absence of the intracellular protein calnexin. In addition, 10% of each lysate was denatured and loaded onto separate gels. Immunoblotting for calnexin on the membranes of lysate was done to confirm uniform protein loading.
Densitometry analysis (Image Lab BioRad software) was used to estimate the relative total amount of L, M and S mutant proteins, which were expressed relative of the wild type L, M and S total proteins.

Flow cytometry. The surface expression of NTCP, ERp46, ERp57 and ERp72 was quantified by FACS analysis from 10^6 live cells using antibodies added to cells for 1h at 4°C. After washing, the binding of antibody to the cell surface was detected using PE (Phycoerythrin)-conjugated anti-mouse antibodies.

Immuno-fluorescence (IF), confocal microscopy imaging and image analysis. Huh7-NTCP cells were grown on uncoated 14mm-diameter glass coverslips. Forty-eight hours after seeding, cells were washed with PBS, fixed with 3% paraformaldehyde in PBS for 15 min, quenched with 50mM NH4Cl and permeabilized with 0.1% Triton X-100 for 7min. Fixed cells were then incubated for 1h with primary antibodies in 1% BSA/PBS, washed and stained for 1 hr with the corresponding fluorescent Alexa Fluor conjugated secondary antibody (Alexa-Fluor-488 and Alexa-Fluor-568, Thermo Fisher) in 1% BSA/PBS. Cells were washed three times with PBS, stained for nuclei with Hoechst 33342 (Thermo Fisher) for 5 min, washed two times with PBS and mounted in Mowiol 40-88 (Sigma-Aldrich) prior to image acquisition with LSM-710 confocal microscope (Zeiss). Single section confocal images of 0.6µm of thickness were analyzed with the ImageJ software. The Pearson's correlation coefficients were calculated by using the JACoP plugin for ImageJ.

Cytotoxicity assay. The release of LDH from damaged cells was measured with CytoTox-ONE (Promega, MA, USA) homogeneous membrane integrity assay. Cells were grown in a 96-well flat-bottom culture plate in density of $3x10^3$ cells per well and treated with the different drugs for 2h or 24h. Maximum LDH release was determined by adding 2µl of CytoTox-ONE lysis solution to control wells for 10min. The assay was performed in 96-well plates by adding 100 µl of the sample supernatant and 100 µl of CytoTox-ONE reagent, after which the plate was shaken for 10s. After 10min of incubation, 50 µl CytoTox-One stop solution was added and the plate was shaken again for 10s. The fluorescence signal was measured at λ_{EX}=560 nm, λ_{EM}=590. LDH-release was calculated as percentage of LDH released in the culture media of total LDH (media and lysates).

Fusion peptide prediction. The HBV surface sequence used was taken from the UniProt database, with accession number P03138. Hydropathy plots were obtained with Membrane Protein eXplorer software (Snider et al., 2009) using as input the reference sequence. Hydropathy plots were also used to evaluate the effect of residue mutations. Sequences with a propensity to partition into the lipid bilayer were identified using interfacial settings and pH=5.0.

Contact prediction on the Cys rich region. Contact prediction was performed using RaptorX (Wang et al., 2017, Teppa et al., 2020). RaptorX integrates evolutionary coupling and sequence conservation information through an ultra-deep neural network formed by two deep residual neural networks. RaptorX predicts pairs of residues, whose mutations have arisen simultaneously during evolution.

Structural models and molecular dynamic simulation studies. The HBV surface protein sequence was taken from the UniProt database, with accession number P03138. Secondary structure prediction was performed with Jpred (Cole et al., 2008). The S protein region 294-317 was modelled using MODELLER (Sali and Blundell, 1993). The template crystal structure of the Newcastle disease virus fusion protein (PDB code: 1G5G) was retrieved from the PDB database (Berman et al., 2000). Sequence alignment was generated with Clustal X (Larkin et al., 2007). The model evaluation was conducted using the Ramachandran plot (Ramachandran et al., 1963). The model of the wild-type sequence was further used to create two structural models with mutations using UCSF Chimera package (Pettersen et al., 2004). One model contains the double mutations T303C/G308C, which may create an extra disulfide bond. The overall effect of those mutations would be to "shift" the disulfide bridge of two amino acids towards the turn of the β-hairpin motif. After mutations, the models were energy minimized by applying Molecular Modelling Toolkit (MMTK) with Amber parameters for standard residues, and 100 steepest descent minimization steps with a step size of 0.02 Å. To investigate the stability of the disulfide bonds, molecular dynamic (MD) simulations of the three models were carried out by GROMACS version 2020 (Abraham et al., 2015) in conjunction with OPLS-AA/L all-atom force field. The models were immersed in the cubic boxes filled with water molecules with a minimal distance of 1.0 nm between the peptide surface and box. Each system was equilibrated to the desired temperature through a stepwise heating protocol in NVT ensemble followed by 100.0 ps equilibration in NPT ensemble with position restraints on the protein molecule. The final productive MD was performed for each system for 10 ns under periodic boundary conditions without any restraints on the protein with a time step of 2 fs at constant pressure (1 atm) and temperature (300 K). Coordinates were saved every 10 ps, yielding 1000 frames per MD trajectory. All the frames were further investigated to differentiate between allosteric and structurally stabilizing disulfides. Disulfide bonds were classified based on the five relevant torsion angles (χ_1, χ_2, χ_3, $\chi_{2'}$ and $\chi_{1'}$) (see Figure 4-figure

supplement 2), disulfides were treated as symmetrical. In this system, twenty conformational categories are possible (Marques et al., 2010; Schmidt and Hogg, 2007; Schmidt et al., 2006). The three central angles (χ_2, χ_3 and χ_2) define the basic shape: Spiral, Hook and Staple (Eklund et al., 1984). The χ_3 defines the orientationally motif: left-handed (LH) or right-handed (RH) if the sign is negative or positive, respectively (Eklund et al., 1984). The χ_1 and $\chi_{1'}$ determines the sign of the nomenclature (Qi and Grishin, 2005).

***In vivo* experiments.** All experiments were performed in accordance with the European Union guidelines for approval of the protocols by the local ethics committee (Authorization Agreement C2EA-15, "Comité Rhône-Alpes d'Ethique pour l'Expérimentation Animale", Lyon, France - APAFIS#27316-2020060810332115 v4). Primary human hepatocytes (PHH, Corning, BD Gentest) were intrasplenically injected in NFRG mice (Azuma et al., 2007), a triple mutant mouse knocked-out for fumarylacetoacetate hydrolase ($fah^{-/-}$), recombinase activating gene 2 ($rag2^{-/-}$), interleukin 2 receptor gamma chain ($IL2rg^{-/-}$). 48h after adeno-uPA conditioning (Bissig et al., 2010; Calattini et al., 2015). Mice were subjected to NTBC cycling during the liver repopulation process, as described previously (Calattini et al., 2015). Mice with human serum albumin (HSA) levels >15 mg/mL, as determined using a Cobas C501 analyzer (Roche Applied Science), were inoculated with virus preparations by intra-peritoneal injection. Sera were collected at different time points before and after infection. Mice were sacrificed 6 weeks post-infection.

Statistical analysis. Statistical analyses were performed using GraphPad Prism version 5.02 for Windows, GraphPad Software (San Diego California, USA). The Mann-Whitney or Wilcoxon tests were used for statistical comparisons. A p-value of 0.05 or less was considered as significant. When applicable, data are presented as mean ± standard deviation and results of the statistical analysis are shown as follows: ns, not significant ($P > 0.05$); *, $P < 0.05$; **, $P < 0.01$; and ***, $P < 0.001$.

Acknowledgment

We are grateful to Camille Sureau for the HBV GP expression constructs and for sharing the HDV infection assay. We thank Solène Denolly for helpful discussions.

We thank the "Plateforme de Thérapie Génique" in Nantes (France) for the production of the *in vivo*-certified lots of adeno-uPA vectors. We thank Jean-François Henry, Nadine Aguilera and Tiphaine Dorel from the animal facility (PBES, Plateau de Biologie Experimental de la Souris, UMS3444/CNRS, US8/Inserm, ENS de Lyon, UCBL), and Véronique Pierre for her technical help in handling of mice. We acknowledge the contribution of the ANIRA-Genetic Analysis and the PLATIM-Microscopy

facilities of SFR Biosciences (UMS3444/CNRS, US8/Inserm, ENS de Lyon, UCBL) for images quantifications, technical assistance and support. We thank Didier Décimo for support with the BSL3 facility. We thank Didier Décimo for support with the BSL3 facility. We thank Omran Allatif for guidance with the statistical analysis.

Funding

This work was supported by the French ‘‘Agence Nationale de la Recherche sur le SIDA et les Hépatites Virales | Maladie Infectieuses Emergentes” (ANRS|MIE, grants ECTZ71388, ECTZ160643, ECTZ160726, ECTZ38814 and ECTZ41733), the Foundation FINOVI, the 2017 Call for Joriss Projects, the LabEx Ecofect (ANR-11-LABX-0048) of the ‘‘Université de Lyon”, within the program ‘‘Investissements d’Avenir” (ANR-11-IDEX-0007) operated by the French National Research Agency (ANR), and the LabEX CALSIMLAB (ANR-11-LABX-0037-01 and ANR-11-IDEX-0004-02).

Competing interests

The authors have declared that no competing interests exist.

References

Abell, B.A., and Brown, D.T. (1993). Sindbis virus membrane fusion is mediated by reduction of glycoprotein disulfide bridges at the cell surface. J. Virol. *67*, 5496–5501.

Abou-Jaoudé, G., and Sureau, C. (2007). Entry of hepatitis delta virus requires the conserved cysteine residues of the hepatitis B virus envelope protein antigenic loop and is blocked by inhibitors of thiol-disulfide exchange. J. Virol. *81*, 13057–13066.

Abraham, M.J., Murtola, T., Schulz, R., Páll, S., Smith, J.C., Hess, B., and Lindahl, E. (2015). GROMACS: High performance molecular simulations through multi-level parallelism from laptops to supercomputers. SoftwareX *1-2*, 19–25.

Apellániz, B., Huarte, N., Largo, E., and Nieva, J.L. (2014). The three lives of viral fusion peptides. Chemistry and Physics of Lipids *181*, 40–55.

757 Azuma, H., Paulk, N., Ranade, A., Dorrell, C., Al-Dhalimy, M., Ellis, E., Strom, S., Kay, M.A., Finegold,
758 M., and Grompe, M. (2007). Robust expansion of human hepatocytes in Fah−/−/Rag2−/−/Il2rg−/−
759 mice. Nature Biotechnology *25*, 903–910.

760 Barbouche, R., Miquelis, R., Jones, I.M., and Fenouillet, E. (2003). Protein-disulfide isomerase-
761 mediated reduction of two disulfide bonds of HIV envelope glycoprotein 120 occurs post-CXCR4
762 binding and is required for fusion. J Biol Chem *278*, 3131–3136.

763 Baumert, T.F., Meredith, L., Ni, Y., Felmlee, D.J., McKeating, J.A., and Urban, S. (2014). Entry of
764 hepatitis B and C viruses - recent progress and future impact. Curr Opin Virol *4*, 58–65.

765 Berman, H.M., Bhat, T.N., Bourne, P.E., Feng, Z., Gilliland, G., Weissig, H., and Westbrook, J. (2000).
766 The Protein Data Bank and the challenge of structural genomics. Nat. Struct. Biol. *7 Suppl*, 957–959.

767 Berting, A., Fischer, C., Schaefer, S., Garten, W., Klenk, H.D., and Gerlich, W.H. (2000). Hemifusion
768 activity of a chimeric influenza virus hemagglutinin with a putative fusion peptide from hepatitis B virus.
769 Virus Res *68*, 35–49.

770 Bissig, K.-D., Wieland, S.F., Tran, P., Isogawa, M., Le, T.T., Chisari, F.V., and Verma, I.M. (2010).
771 Human liver chimeric mice provide a model for hepatitis B and C virus infection and treatment. J Clin
772 Invest *120*, 924–930.

773 Blanchet, M., and Sureau, C. (2007). Infectivity determinants of the hepatitis B virus pre-S domain are
774 confined to the N-terminal 75 amino acid residues. J. Virol. *81*, 5841–5849.

775 Bremer, C.M., Bung, C., Kott, N., Hardt, M., and Glebe, D. (2009). Hepatitis B virus infection is
776 dependent on cholesterol in the viral envelope. Cell. Microbiol. *11*, 249–260.

777 Bremer, C.M., Sominskaya, I., Skrastina, D., Pumpens, P., El Wahed, A.A., Beutling, U., Frank, R.,
778 Fritz, H.-J., Hunsmann, G., Gerlich, W.H., et al. (2011). N-terminal myristoylation-dependent masking
779 of neutralizing epitopes in the preS1 attachment site of hepatitis B virus. Journal of Hepatology *55*,
780 29–37.

781 Calattini, S., Fusil, F., Mancip, J., Dao Thi, V.L., Granier, C., Gadot, N., Scoazec, J.-Y., Zeisel, M.B.,
782 Baumert, T.F., Lavillette, D., et al. (2015). Functional and Biochemical Characterization of Hepatitis C
783 Virus (HCV) Particles Produced in a Humanized Liver Mouse Model. J. Biol. Chem. *290*, 23173–
784 23187.

785 Chiu, J., and Hogg, P.J. (2019). Allosteric disulfides: Sophisticated molecular structures enabling
786 flexible protein regulation. J. Biol. Chem. *294*, 2949–2960.

787 Chojnacki, J., Anderson, D.A., and Grgacic, E.V.L. (2005). A hydrophobic domain in the large
788 envelope protein is essential for fusion of duck hepatitis B virus at the late endosome. J Virol *79*,
789 14945–14955.

790 Cole, C., Barber, J.D., and Barton, G.J. (2008). The Jpred 3 secondary structure prediction server.
791 Nucleic Acids Res. *36*, W197–W201.

792 Delgado, C.L., Núñez, E., Yélamos, B., Gómez-Gutiérrez, J., Peterson, D.L., and Gavilanes, F.
793 (2012). Spectroscopic characterization and fusogenic properties of preS domains of duck hepatitis B
794 virus. Biochemistry *51*, 8444–8454.

795 Delos, S.E., and White, J.M. (2000). Critical role for the cysteines flanking the internal fusion peptide
796 of avian sarcoma/leukosis virus envelope glycoprotein. J Virol *74*, 9738–9741.

797 Delos, S.E., Gilbert, J.M., and White, J.M. (2000). The central proline of an internal viral fusion peptide
798 serves two important roles. J Virol *74*, 1686–1693.

799 Diwaker, D., Mishra, K.P., and Ganju, L. (2013). Potential roles of protein disulphide isomerase in viral
800 infections. Acta Virol. *57*, 293–304.

801 Earp, L.J., Delos, S.E., Park, H.E., and White, J.M. (2004). The Many Mechanisms of Viral Membrane
802 Fusion Proteins. In Membrane Trafficking in Viral Replication, M. Marsh, ed. (Berlin, Heidelberg:
803 Springer Berlin Heidelberg), pp. 25–66.

804 Eklund, H., Cambillau, C., Sjöberg, B.M., Holmgren, A., Jörnvall, H., Höög, J.O., and Brändén, C.I.
805 (1984). Conformational and functional similarities between glutaredoxin and thioredoxins. EMBO J. *3*,
806 1443–1449.

807 Epand, R.M. (2003). Fusion peptides and the mechanism of viral fusion. Biochimica et Biophysica
808 Acta (BBA) - Biomembranes *1614*, 116–121.

809 Fenouillet, E., Barbouche, R., and Jones, I.M. (2007). Cell entry by enveloped viruses: redox
810 considerations for HIV and SARS-coronavirus. Antioxid. Redox Signal. *9*, 1009–1034.

811 Freitas, N., Enguehard, M., Denolly, S., Levy, C., Neveu, G., Lerolle, S., Devignot, S., Weber, F.,
812 Bergeron, E., Legros, V., et al. (2020). The interplays between Crimean-Congo hemorrhagic fever

virus (CCHFV) M segment-encoded accessory proteins and structural proteins promote virus assembly and infectivity. PLoS Pathog. *16*, e1008850.

Glebe, D., Urban, S., Knoop, E.V., Cag, N., Krass, P., Grün, S., Bulavaite, A., Sasnauskas, K., and Gerlich, W.H. (2005). Mapping of the hepatitis B virus attachment site by use of infection-inhibiting preS1 lipopeptides and tupaia hepatocytes. Gastroenterology *129*, 234–245.

Grgacic, E.V., and Schaller, H. (2000). A metastable form of the large envelope protein of duck hepatitis B virus: low-pH release results in a transition to a hydrophobic, potentially fusogenic conformation. J Virol *74*, 5116–5122.

Gripon, P., Cannie, I., and Urban, S. (2005). Efficient inhibition of hepatitis B virus infection by acylated peptides derived from the large viral surface protein. J. Virol. *79*, 1613–1622.

Harrison, S.C. (2015). Viral membrane fusion. Virology *479-480*, 498–507.

van Hemert, F.J., Zaaijer, H.L., Berkhout, B., and Lukashov, V.V. (2008). Mosaic amino acid conservation in 3D-structures of surface protein and polymerase of hepatitis B virus. Virology *370*, 362–372.

Herrscher, C., Pastor, F., Burlaud - Gaillard, J., Dumans, A., Seigneuret, F., Moreau, A., Patient, R., Eymieux, S., Rocquigny, H., Hourioux, C., et al. (2020). Hepatitis B virus entry into HEPG2-NTCP cells requires clathrin-mediated endocytosis. Cellular Microbiology *22*.

Hogg, P.J. (2003). Disulfide bonds as switches for protein function. Trends Biochem. Sci. *28*, 210–214.

Hogg, P.J. (2013). Targeting allosteric disulphide bonds in cancer. Nature Reviews Cancer *13*, 425–431.

Huang, H.-C., Chen, C.-C., Chang, W.-C., Tao, M.-H., and Huang, C. (2012). Entry of Hepatitis B Virus into Immortalized Human Primary Hepatocytes by Clathrin-Dependent Endocytosis. Journal of Virology *86*, 9443–9453.

Iwamoto, M., Saso, W., Sugiyama, R., Ishii, K., Ohki, M., Nagamori, S., Suzuki, R., Aizaki, H., Ryo, A., Yun, J.-H., et al. (2019). Epidermal growth factor receptor is a host-entry cofactor triggering hepatitis B virus internalization. Proceedings of the National Academy of Sciences *116*, 8487–8492.

840 Jain, S., McGinnes, L.W., and Morrison, T.G. (2007). Thiol/disulfide exchange is required for
841 membrane fusion directed by the Newcastle disease virus fusion protein. J. Virol. *81*, 2328–2339.

842 Key, T., Sarker, M., de Antueno, R., Rainey, J.K., and Duncan, R. (2015). The p10 FAST protein
843 fusion peptide functions as a cystine noose to induce cholesterol-dependent liposome fusion without
844 liposome tubulation. Biochim. Biophys. Acta *1848*, 408–416.

845 Komla-Soukha, I., and Sureau, C. (2006). A tryptophan-rich motif in the carboxyl terminus of the small
846 envelope protein of hepatitis B virus is central to the assembly of hepatitis delta virus particles. J Virol
847 *80*, 4648–4655.

848 Korba, B.E., Montero, A.B., Farrar, K., Gaye, K., Mukerjee, S., Ayers, M.S., and Rossignol, J.-F.
849 (2008). Nitazoxanide, tizoxanide and other thiazolides are potent inhibitors of hepatitis B virus and
850 hepatitis C virus replication. Antiviral Research *77*, 56–63.

851 Larkin, M.A., Blackshields, G., Brown, N.P., Chenna, R., McGettigan, P.A., McWilliam, H., Valentin, F.,
852 Wallace, I.M., Wilm, A., Lopez, R., et al. (2007). Clustal W and Clustal X version 2.0. Bioinformatics
853 *23*, 2947–2948.

854 Lavillette, D., Bartosch, B., Nourrisson, D., Verney, G., Cosset, F.-L., Penin, F., and Pécheur, E.-I.
855 (2006). Hepatitis C virus glycoproteins mediate low pH-dependent membrane fusion with liposomes. J.
856 Biol. Chem. *281*, 3909–3917.

857 Lavillette, D., Pécheur, E.-I., Donot, P., Fresquet, J., Molle, J., Corbau, R., Dreux, M., Penin, F., and
858 Cosset, F.-L. (2007). Characterization of fusion determinants points to the involvement of three
859 discrete regions of both E1 and E2 glycoproteins in the membrane fusion process of hepatitis C virus.
860 J. Virol. *81*, 8752–8765.

861 Le Duff, Y., Blanchet, M., and Sureau, C. (2009). The pre-S1 and antigenic loop infectivity
862 determinants of the hepatitis B virus envelope proteins are functionally independent. J. Virol. *83*,
863 12443–12451.

864 Leistner, C.M., Gruen-Bernhard, S., and Glebe, D. (2008). Role of glycosaminoglycans for binding and
865 infection of hepatitis B virus. Cell Microbiol *10*, 122–133.

866 Le Seyec, J., Chouteau, P., Cannie, I., Guguen-Guillouzo, C., and Gripon, P. (1999). Infection Process
867 of the Hepatitis B Virus Depends on the Presence of a Defined Sequence in the Pre-S1 Domain.
868 Journal of Virology *73*, 2052–2057.

Lin, A.H., and Cannon, P.M. (2002). Use of pseudotyped retroviral vectors to analyze the receptor-binding pocket of hemagglutinin from a pathogenic avian influenza A virus (H7 subtype). Virus Res *83*, 43–56.

Ma, J., Wang, S., Wang, Z., and Xu, J. (2015). Protein contact prediction by integrating joint evolutionary coupling analysis and supervised learning. Bioinformatics *31*, 3506–3513.

Macovei, A., Radulescu, C., Lazar, C., Petrescu, S., Durantel, D., Dwek, R.A., Zitzmann, N., and Nichita, N.B. (2010). Hepatitis B virus requires intact caveolin-1 function for productive infection in HepaRG cells. J. Virol. *84*, 243–253.

Macovei, A., Petrareanu, C., Lazar, C., Florian, P., and Branza-Nichita, N. (2013). Regulation of hepatitis B virus infection by Rab5, Rab7, and the endolysosomal compartment. J. Virol. *87*, 6415–6427.

Mangold, C.M., Unckell, F., Werr, M., and Streeck, R.E. (1995). Secretion and antigenicity of hepatitis B virus small envelope proteins lacking cysteines in the major antigenic region. Virology *211*, 535–543.

Marques, J.R.F., da Fonseca, R.R., Drury, B., and Melo, A. (2010). Conformational characterization of disulfide bonds: A tool for protein classification. Journal of Theoretical Biology *267*, 388–395.

Martin, I., Ruysschaert, J.-M., and Epand, R.M. (1999). Role of the N-terminal peptides of viral envelope proteins in membrane fusion. Adv Drug Deliv Rev *38*, 233–255.

Müller, J., Naguleswaran, A., Müller, N., and Hemphill, A. (2008). Neospora caninum: Functional inhibition of protein disulfide isomerase by the broad-spectrum anti-parasitic drug nitazoxanide and other thiazolides. Experimental Parasitology *118*, 80–88.

Ni, Y., Sonnabend, J., Seitz, S., and Urban, S. (2010). The Pre-S2 Domain of the Hepatitis B Virus Is Dispensable for Infectivity but Serves a Spacer Function for L-Protein-Connected Virus Assembly. Journal of Virology *84*, 3879–3888.

Ni, Y., Lempp, F.A., Mehrle, S., Nkongolo, S., Kaufman, C., Fälth, M., Stindt, J., Königer, C., Nassal, M., Kubitz, R., et al. (2014). Hepatitis B and D viruses exploit sodium taurocholate co-transporting polypeptide for species-specific entry into hepatocytes. Gastroenterology *146*, 1070–1083.

Pacello, F., D'Orazio, M., and Battistoni, A. (2016). An ERp57-mediated disulphide exchange promotes the interaction between Burkholderia cenocepacia and epithelial respiratory cells. Sci Rep *6*, 21140.

Perez-Vargas, J., Amirache, F., Boson, B., Mialon, C., Freitas, N., Sureau, C., Fusil, F., and Cosset, F.-L. (2019). Enveloped viruses distinct from HBV induce dissemination of hepatitis D virus in vivo. Nature Communications *10*.

Pettersen, E.F., Goddard, T.D., Huang, C.C., Couch, G.S., Greenblatt, D.M., Meng, E.C., and Ferrin, T.E. (2004). UCSF Chimera--a visualization system for exploratory research and analysis. J Comput Chem *25*, 1605–1612.

Qi, Y., and Grishin, N.V. (2005). Structural classification of thioredoxin-like fold proteins. Proteins *58*, 376–388.

Ramachandran, G.N., Ramakrishnan, C., and Sasisekharan, V. (1963). Stereochemistry of polypeptide chain configurations. Journal of Molecular Biology *7*, 95–99.

Rey, F.A., and Lok, S.-M. (2018). Common Features of Enveloped Viruses and Implications for Immunogen Design for Next-Generation Vaccines. Cell *172*, 1319–1334.

Richard, C., Liuzzo, J.P., and Moscatelli, D. (1995). Fibroblast Growth Factor-2 Can Mediate Cell Attachment by Linking Receptors and Heparan Sulfate Proteoglycans on Neighboring Cells. Journal of Biological Chemistry *270*, 24188–24196.

Rigg, R.J., and Schaller, H. (1992). Duck hepatitis B virus infection of hepatocytes is not dependent on low pH. J. Virol. *66*, 2829–2836.

Rodríguez-Crespo, I., Gómez-Gutiérrez, J., Nieto, M., Peterson, D.L., and Gavilanes, F. (1994). Prediction of a putative fusion peptide in the S protein of hepatitis B virus. J Gen Virol *75 (Pt 3)*, 637–639.

Rodríguez-Crespo, I., Núñez, E., Gómez-Gutiérrez, J., Yélamos, B., Albar, J.P., Peterson, D.L., and Gavilanes, F. (1995). Phospholipid interactions of the putative fusion peptide of hepatitis B virus surface antigen S protein. J Gen Virol *76 (Pt 2)*, 301–308.

Rodríguez-Crespo, I., Núñez, E., Yélamos, B., Gómez-Gutiérrez, J., Albar, J.P., Peterson, D.L., and Gavilanes, F. (1999). Fusogenic activity of hepadnavirus peptides corresponding to sequences downstream of the putative cleavage site. Virology *261*, 133–142.

925 Rosenthal, P.B., Zhang, X., Formanowski, F., Fitz, W., Wong, C.H., Meier-Ewert, H., Skehel, J.J., and
926 Wiley, D.C. (1998). Structure of the haemagglutinin-esterase-fusion glycoprotein of influenza C virus.
927 Nature *396*, 92–96.

928 Ruiz-Olmedo, M.I., González-Hernández, I., Palomares-Alonso, F., Franco-Pérez, J., González F., M.
929 de L., and Jung-Cook, H. (2017). Effect of nitazoxanide on albendazole pharmacokinetics in
930 cerebrospinal fluid and plasma in rats. Saudi Pharmaceutical Journal *25*, 413–418.

931 Sali, A., and Blundell, T.L. (1993). Comparative protein modelling by satisfaction of spatial restraints.
932 J. Mol. Biol. *234*, 779–815.

933 Salisse, J., and Sureau, C. (2009). A Function Essential to Viral Entry Underlies the Hepatitis B Virus
934 “a” Determinant. Journal of Virology *83*, 9321–9328.

935 Schmidt, B., and Hogg, P.J. (2007). Search for allosteric disulfide bonds in NMR structures. BMC
936 Struct. Biol. *7*, 49.

937 Schmidt, B., Ho, L., and Hogg, P.J. (2006). Allosteric disulfide bonds. Biochemistry *45*, 7429–7433.

938 Schulze, A., Gripon, P., and Urban, S. (2007). Hepatitis B virus infection initiates with a large surface
939 protein-dependent binding to heparan sulfate proteoglycans. Hepatology *46*, 1759–1768.

940 Siegler, V.D., and Bruss, V. (2013). Role of transmembrane domains of hepatitis B virus small surface
941 proteins in subviral-particle biogenesis. J Virol *87*, 1491–1496.

942 Snider, C., Jayasinghe, S., Hristova, K., and White, S.H. (2009). MPEx: a tool for exploring membrane
943 proteins. Protein Sci. *18*, 2624–2628.

944 Stockis, A., Deroubaix, X., Lins, R., Jeanbaptiste, B., Calderon, P., and Rossignol, J.F. (1996).
945 Pharmacokinetics of nitazoxanide after single oral dose administration in 6 healthy volunteers.
946 International Journal of Clinical Pharmacology and Therapeutics *34*, 349–351.

947 Sureau, C. (2010). The use of hepatocytes to investigate HDV infection: the HDV/HepaRG model.
948 Methods Mol. Biol. *640*, 463–473.

949 Sureau, C., Guerra, B., and Lee, H. (1994). The middle hepatitis B virus envelope protein is not
950 necessary for infectivity of hepatitis delta virus. J. Virol. *68*, 4063–4066.

951 Turano, C., Coppari, S., Altieri, F., and Ferraro, A. (2002). Proteins of the PDI family: unpredicted non-
952 ER locations and functions. J. Cell. Physiol. *193*, 154–163.

Wang, S., Sun, S., Li, Z., Zhang, R., and Xu, J. (2017). Accurate De Novo Prediction of Protein Contact Map by Ultra-Deep Learning Model. PLoS Comput. Biol. *13*, e1005324.

White, J.M., and Whittaker, G.R. (2016). Fusion of Enveloped Viruses in Endosomes. Traffic *17*, 593–614.

Wouters, M.A., Lau, K.K., and Hogg, P.J. (2004). Cross-strand disulphides in cell entry proteins: poised to act. Bioessays *26*, 73–79.

Yan, H., Zhong, G., Xu, G., He, W., Jing, Z., Gao, Z., Huang, Y., Qi, Y., Peng, B., Wang, H., et al. (2012). Sodium taurocholate cotransporting polypeptide is a functional receptor for human hepatitis B and D virus. Elife *1*, e00049.

Yan, H., Liu, Y., Sui, J., and Li, W. (2015). NTCP opens the door for hepatitis B virus infection. Antiviral Res. *121*, 24–30.

Zhou, B., Baldus, I.B., Li, W., Edwards, S.A., and Gräter, F. (2014). Identification of allosteric disulfides from prestress analysis. Biophys. J. *107*, 672–681.

Figure legends

Figure 1. HBV GP fusion trigger is independent of acid pH, HSPG and NTCP. (**A**) Huh7 "donor" cells transfected with the pT7HB2.7 plasmid allowing expression of HBV GPs (HBV) and a luciferase marker gene driven by the HIV-1 promoter were co-cultured with either Huh7-tat (H-tat) or Huh7-NTCP-tat (N-tat) "indicator" cells that express the HIV Tat protein. After 24h of co-culture, the cells were treated at pH4 (or pH 5 for VSV-G) *vs*. pH7 for 3 minutes. The luciferase activity induced by fusion between donor and indicator cells was then measured 24h later. A control plasmid that does not allow GP expression (Empty) was used to determine the background of luciferase expression. The CCHFV Gn/Gc (CCHFV) or VSV-G (VSV) GPs were used as positive controls for fusion at low pH. Fusion mediated by HBV GPs with Huh7-tat cells was taken as 100%. The bars represent the means (N=3). Error bars correspond to standard deviation. See the raw data of individual experiments in Figure 1-figure supplement 1. (**B**) Results of cell-cell fusion assays performed as above-described in the presence of heparin at the indicated concentrations throughout the co-coculture. No cytotoxicity could be detected in these conditions (Figure 1-figure supplement 2). The graphs represent the average of two independent experiments. Fusion mediated by HBV GPs with mock-treated Huh7 cells was taken as 100%. (**C**) CHO "donor" cells transfected with the pT7HB2.7 plasmid and a luciferase marker gene driven by the HIV-1 promoter were co-cultured with either Huh7-tat (H-tat), CHO-tat (CHO wt), or CHO-pgsB618-tat (pgsB618) "indicator" cells that express the HIV Tat protein. The luciferase activity induced by fusion between donor and indicator cells was then measured 24h later. A control plasmid that does not allow GP expression (Empty) was used to determine the background of luciferase expression. Fusion mediated by HBV GPs with Huh7-tat was taken as 100%. The graphs represent the average of two independent experiments. (**D**) Huh7 "donor" cells transfected plasmids allowing expression of L, M or S HBV GPs alone, both L and S GPs (noM) or all HBV GPs (Wt) and a luciferase marker gene driven by the HIV-1 promoter were co-cultured with Huh7-tat or Huh7-NTCP-tat "indicator" cells that express HIV Tat protein. Cell co-cultures were then processed as above described to determine cell-cell fusion activity. Fusion mediated by HBV GP at pH7 with Huh7-tat cells was taken as 100%. The bars represent the means (N=3). Error bars correspond to standard deviation. (**E**) Detection of HBV GPs at the cell surface by biotinylation. Transfected Huh7 cells were biotinylated for 30 min at 4°C and then processed biochemically. Cell lysates were subjected to streptavidin pull-down prior to western blot analysis using anti-HBsAg antibody (Murex). The molecular weight markers (kDa) are shown to the right. Calnexin detection was used as control for cytoplasmic protein marker, showing the integrity of cell membrane, as shown in this representative western blot. (**F**) Relative GPs expression at the cell surface as compared to Wt, quantified by adding the L+M+S signals from western blot analyses. The results are expressed as mean ± SD (N=3). No statistical

differences could be found using the Mann-Whitney test (p-value >0.05). See also the quantification of total HBV GP expression in the Figure 1-figure supplement 4.

Figure 2. Functional analysis of predicted HBV fusion peptides. (**A**) Sequence of HBV L protein showing the amino acid color code and boxes for the localization of the two predicted fusion peptides in preS1 and in preS2. (**B**) Sequence of the two predicted fusion peptides showing the positions that were mutated (bold)**.** (**C, D**) Huh7 cells were co-transfected with pSVLD3 plasmid coding for HDV RNPs and plasmids coding for wt or mutant HBV GPs. The FW/AA and FW/EE are double alanine mutants at position F52 and W66. As control, pSVLD3 was co-transfected with an empty plasmid (referred to as "noGP"). At day 9 post-transfection, the cell supernatants were harvested, filtered and the extracellular RNA was extracted and purified before quantifying HDV RNAs by RTqPCR HDV RNA levels in GE (genome equivalent) are expressed as means ± SD (N=3) per mL of cell supernatants. (**E, F**) HDV particles were used to infect Huh7-NTCP cells, which were grown for 7 days before total intracellular RNA was purified. The results of HDV RNA quantification by RTqPCR are expressed after normalization with GAPDH RNAs as means ± SD (N=3) per mL of cell lysates containing 10^6 cells. (**G, H**) Huh7 "donor" cells co-expressing wt or mutant HBV GPs and a luciferase marker gene driven by the HIV-1 promoter were co-cultured with either Huh7-tat (H-tat) or Huh7-NTCP-tat (N-tat) "indicator" cells that express HIV Tat protein. After 24h, the cells were treated at pH4 or pH7 for 3 minutes. The luciferase activity induced by the fusion between the donor and indicator cells was measured 24h later. Fusion mediated by wt GP at pH7 with Huh7-NTCP-tat cells was taken as 100%. The bars represent the means (N=5). Error bars correspond to standard deviations. (**I, J**) Quantification of wt and mutant GPs at cell surface by western blot analyses (see examples in Figure 2-figure supplement 2). The results show the relative GPs expression of preS1 (I) and preS2 (J) mutants compared to Wt, as indicated, and are expressed as means ± SD (N=3). No statistical differences could be found using the Mann-Whitney test (p-value >0.05).

Figure 3. DTNB, a thiol-specific oxidizing reagent, inhibits HBV membrane fusion. (**A**) DTNB (2 mM) was added to the cell supernatant containing HDV particles at the onset of infection (0h) or at the indicated times post-infection and was removed 8hr later. VSV-Δp, *i.e.*, HDV particles generated with VSV-G GP rather than HBV, were used as control for a virus entry process that is not affected by DNTB. As negative control, pSVLD3 was co-transfected with an empty plasmid (referred to as "noGP"). At 7 days post-infection, HDV RNAs were extracted from infected cells and quantified by RTqPCR. The results are expressed after normalization with GAPDH RNAs as means ± SD (N=3) per mL of cell lysates containing 10^6 cells. The results of infection in the absence of DTNB are shown [DTNB(-)]. (**B**) Huh7 "donor" cells co-expressing HBV GPs and a luciferase marker gene driven by the HIV-1 promoter were co-cultured with Huh7-NTCP-tat "indicator" cells that express HIV Tat protein.

Different concentrations of DTNB were added at 0h *vs*. at 16h after initiating the cell co-culture, as indicated. No cytotoxicity could be detected in these conditions (Figure 1-figure supplement 2). The luciferase activity induced by fusion between donor and indicator cells was then measured 24h later. Fusion mediated by HBV GPs without DTNB was taken as 100%. The graphs represent the average of four independent experiments. (**C, D**) Huh7 cells transfected with pUC19 (noGP) or the pT7HB2.7 (HBV) plasmids were incubated with DMSO (0) or increasing doses of DTNB (0.5, 1 and 2 mM) for 16h prior to incubation with biotin for 30 min at 4°C. Biotin was omitted from one sample (-) and served as a negative control for non-specific binding of proteins to streptavidin. Cells were subsequently lysed and the biotinylated surface proteins were captured by streptavidin agarose. Total (**C**) and biotin-labelled proteins (**D**) were then analyzed by western blot using anti-HBsAg (Murex) and anti-calnexin antibodies. Calnexin detection was used as control for cytoplasmic protein marker, showing the integrity of cell membrane, as shown in these representative western blots. The molecular weight markers (kDa) are shown to the left.

Figure 4. Disulfides conformation models. (**A**) Cysteine-rich regions on the "a" determinant (residues 261-324) of the HBV S GP. Four sub-regions that are rich in cysteine are coloured: I (blue), II (green), III (yellow) and IV (red). Jpred secondary structure prediction different from random-coil is indicated: β-strand (arrow) and α-helix (zigzag line). (**B**) Probability of contacts predicted by RaptorX between the four cysteine-rich regions. The probabilities higher than 0.7 are highlighted in red (see also Figure 4-figure supplement 1). (**C**) Predominant disulfide conformations obtained by molecular dynamics simulation of the modelled 294-317 region of the HBV surface protein. Note that the ß-strand on the wt sequence (left) adopts a loop conformation with an allosteric disulfide conformer between the C301-C310 bond, which is specifically classified as a -/+RHHook conformation. The T303C/G308C double mutant (right) may generate an additional disulfide bond, resulting in two structural disulfides of +/-RHStaple and -/+LHSpiral conformations that form the C301-310 and C303-C308 bonds, respectively.

Figure 5. **Evidence for a functional role of the CSD in the region 294-317 of the HBV S GP.** (**A)** Huh7 cells were co-transfected with pSVLD3 plasmid coding for HDV RNPs and plasmids coding for wt, single or double mutant (TG/CC) HBV GPs. As control, pSVLD3 was co-transfected with an empty plasmid (referred to as "noGP"). At day 9 post-transfection, the cell supernatants were harvested, filtered and the extracellular RNA was extracted and purified before quantifying HDV RNAs by RTqPCR. HDV RNA levels in GE (genome equivalent) are expressed as means ± SD (N=4) per mL of cell supernatants. (**B**) HDV particles were used to infect Huh7-NTCP cells, which were grown for 7 days before total intracellular RNA was purified. The results of HDV RNA quantification by RTqPCR are expressed after normalization with GAPDH RNAs as means ± SD (N=4) per mL of cell lysates

containing 10^6 cells. (**C**) Detection of GP mutants at the cell surface by biotinylation. Huh7 cells expressing wt or mutant HBV GPs were biotinylated for 30 min at 4°C and then processed biochemically. Cell lysates were subjected to streptavidin pull-down prior to western blot analysis using anti-HBsAg antibody (Murex). The molecular weight markers (kDa) are shown to the left. Calnexin detection was used as control for cytoplasm protein marker, showing the integrity of cell membrane, as shown in this representative western blot. The relative quantification of cell surface GP expression compared to wt were quantified from western blot analyses (means ± SD; N=3) are shown below. See the quantification of total HBV GP expression in the Figure 1-figure supplement 4. (**D**) Huh7 "donor" cells co-expressing wt or mutant HBV GPs and a luciferase marker gene driven by the HIV-1 promoter were co-cultured with either Huh7-tat (H-tat) or Huh7-NTCP-tat (N-tat) "indicator" cells that express HIV Tat protein. After 24h, the cells were treated at pH4 or pH7 for 3 minutes. The luciferase activity induced by the fusion between the donor and indicator cells was measured 24h later. Fusion mediated by wt GP at pH7 with Huh7-NTCP-tat cells was taken as 100%. The bars represent the means (N=4). Error bars correspond to standard deviations.

Figure 6. PDI inhibitors in HBV entry. (**A)** HDV particles harboring wt or TG/CC mutant (T330C/G308C) HBV GPs were incubated with Huh7 or Huh7-NTCP cells that were pre-treated for 2h with the indicated inhibitors that block different PDI proteins or with DMSO, used as vehicle. Binding of either virus particles to the cells was quantified by RTqPCR and expressed after normalization with GAPDH RNAs as mean ± SD (N=3) per mL of cell lysates containing 10^6 cells. (**B)** HDV or (**C**) HBV particles were used to infect Huh7-NTCP cells that were pre-incubated for 2h with the indicated inhibitors that block different PDI proteins or with DMSO, used as vehicle. Infected cells were grown for 7 days before total intracellular RNA or DNA was purified. The results of HDV RNA and HBV DNA quantification by RTqPCR and qPCR, respectively, are expressed after normalization with GAPDH RNAs as means ± SD (N=3) per mL of cell lysates containing 10^6 cells. (**D**) Huh7 "donor" cells co-expressing HBV GPs and a luciferase marker gene driven by the HIV-1 promoter were co-cultured with Huh7-NTCP-tat "indicator" cells that express HIV Tat protein. The indicated PDI inhibitors were added when "donor" and "indicator" cells were mixed for co-cultures and the luciferase activity induced by cell-cell fusion was measured 24h later. DMSO was used as vehicle. Fusion mediated by HBV GPs without inhibitor was taken as 100%. The graphs represent the average of four independent experiments. The PDI inhibitors were used at the following concentrations: NTZ, 30 µg/mL; EGCG, 5 µM; Rutin, 5 µM; Bacitracin, 5 mM; PX-12, 30 µg/mL. No cytotoxicity could be detected in these conditions (Figure 1-figure supplement 2).

Figure 7. ERp57 down-regulation inhibits in HBV entry. (**A**) Intracellular (upper panels) and cell-surface (lower panels) staining of ERp46, ERp57 and ERp72 PDI members. Huh7-NTCP cells were

subjected to flow cytometry analysis, in order to evaluate the expression of the indicated PDIs. Cells stained with secondary antibody only (No primary) were used to provide the background of flow cytometry analyses. (**B**) HDV or (**C**) HBV particles were used to infect Huh7-NTCP cells in which the indicated PDIs were down-regulated by lentiviral vectors carrying shRNA (see Figure 7-figure supplement 1 and Figure 7-figure supplement 2). Naïve Huh7-NTCP cells were used as controls. Infected cells were grown for 7 days before total intracellular RNA or DNA was purified. The results of HDV RNA and HBV DNA quantification by RTqPCR and qPCR, respectively, are expressed after normalization with GAPDH RNAs as means ± SD (N=3) per mL of cell lysates containing 10^6 cells. (**D**) Huh7 "donor" cells co-expressing HBV GPs and a luciferase marker gene driven by the HIV-1 promoter were co-cultured with Huh7-NTCP-tat "indicator" cells that express HIV Tat protein in which the indicated PDI were down-regulated by lentiviral vectors carrying shRNA. After 24h, the cells were treated at pH4 or pH7 for 3 minutes. The luciferase activity induced by the fusion between donor and indicator cells was measured 24h later. Fusion mediated by HBV GPs at pH7 with naïve Huh7-NTCP-tat cells (Ctrl) was taken as 100%. A control plasmid that does not allow GP expression (Empty) was used to determine the background of luciferase expression. The bars represent the means (N=3). Error bars correspond to standard deviations.

Figure 8. Intracellular localization of ERp57 in Huh7-NTCP cells. Huh7-NTCP cells were grown on glass cover slides and fixed 48hrs after seeding. (**A**) Endogenous ERp57 with Rab5, Rab7, Rab11 or Lamp1 were immune-stained, and the colocalization of ERp57 (red channels) with Rab5, Rab7, Rab11 or Lamp1 (green channels) was analyzed by confocal microscopy. Scale bars of panels and zooms from squared area represent 10 µm and 2 µm, respectively. (**B**) The degree of colocalization between ERp57 and the different cell markers was assessed by determining the Pearson's correlation coefficients with the JACoP plugin of ImageJ. Results are expressed as the mean of 6 individual cells. Error bars correspond to standard deviations.

Figure 9. *In vivo* assessment of ERp57 inhibition. (**A**) 4-8 weeks old NOD-FRG mice were engrafted with primary human hepatocytes (PHH). After *ca*. 2-3 months, the animals displaying HSA levels >15 mg/mL were randomly split in 4 different groups (N=3 to N=5 animals, see Table in the inset) that were infected with HBV (10^8 GE/mouse), using the displayed NTZ treatment schedule. (**B**) At different time points post-infection, blood samples (50 µl) were collected and the viremia in sera was monitored by qPCR (GE/mL of serum). The graphs show the results of viremia (means ± SD) of HBV. See results of individual mice in Figure 9-figure supplement 1.

Legends to figure supplements

Figure 1-figure supplement 1. HBV GP fusion trigger is independent of acid pH and NTCP. Huh7 "donor" cells transfected with the pT7HB2.7 plasmid allowing expression of HBV GPs (HBV) and a luciferase marker gene driven by the HIV-1 promoter were co-cultured with either Huh7-tat (H-tat) or Huh7-NTCP-tat (N-tat) "indicator" cells that express the HIV Tat protein. After 24h of co-culture, the cells were treated at pH4 (or pH5 for VSV-G) *vs*. pH7 for 3 minutes. The luciferase activity induced by fusion between donor and indicator cells was then measured 24h later. A control plasmid that does not allow GP expression (Empty) was used to determine the background of luciferase expression. The CCHFV Gn/Gc (CCHFV) or VSV-G GPs (VSV) were used as positive controls for fusion at low pH. Results from three independent experiments expressed as ratios of luciferase activities of the different conditions relative to that of the control conditions.

Figure 1-figure supplement 2. Results of cell survival after drug treatments. The indicated drugs were used as described in Figure 1B (Heparin), Figure 3 (DNTB), and Figure 6 (NTZ, EGCG, Rutin, Bacitracin and PX-12). Cell supernatants were collected immediately after treatment (Post-treatment) or after a further incubation at 37°C of the treated cells (Post-incubation). Cell toxicity assessment was performed with the LDH (CytoTox-ONE Promega) using the indicated positive and negative controls of the kit. Error bars correspond to standard deviations.

Figure 1-figure supplement 3. Characterization of "noM" HDV particles. (**A**) Huh7 cells were co-transfected with pSVLD3 plasmid coding for HDV RNPs and with plasmids encoding either the wt HBV GPs (Wt) or only L and S (noM). As control, pSVLD3 was co-transfected with an empty plasmid (referred to as "noGP"). At day 9 post-transfection, the cell supernatants were harvested, filtered and the extracellular RNA was extracted and purified before quantifying HDV RNAs by RTqPCR. HDV RNA levels in GE (genome equivalent) are expressed as means ± SD (N=4) per mL of cell supernatants. (**B**) HDV or noM particles were used to infect Huh7-NTCP cells, which were grown for 7 days before total intracellular RNA was purified. The results of HDV RNA quantification by RTqPCR, are expressed after normalization with GAPDH RNAs as means ± SD (N=4) per mL of cell lysates containing 10^6 cells.

Figure 1-figure supplement 4. Total protein expression. (**A**) Cell lysates of Huh7 cells expressing the indicated wt or mutant GPs from Figure 1 (left) and Figure 5 (right) were subjected to western blot analysis, using anti-HBsAg antibody (Murex). The molecular weight markers (kDa) are shown to the left. Calnexin detection was used as control for cytoplasmic protein marker, as shown in these representative western blots. The black dots indicate dimers of S, as described in the literature

(Huovila et al., 1992), which are formed in the pre-Golgi compartment (**B**) Relative GPs expression compared to Wt, quantified from western blot using anti-HBsAg antibody. The results are expressed as mean ± SD (N=3).

Figure 2-figure supplement 1. Prediction of fusion peptides within S protein by using Wimley-White Interfacial Hydrophobicity Scale. (**A**) The hydropathy profile (black curve) and its smoothed approximation (green curve). The interface scale measures a residue's free energy of transfer within an unfolded polypeptide chain, from water to a phosphocholine bilayer. The five predicted regions with high propensity to interact with the lipid surface of the cell membrane are indicated with horizontal red bars, the four putative transmembrane regions are indicated with horizontal brown bars. The two regions indicated with red arrows were considered as putative fusogenic peptides. The preS1, preS2 and S regions are represented above the curve. (**B**) Impact of mutations in predicted putative fusogenic segments. The table reports the Gibbs free energy (ΔG) of the two presumed fusogenic segments computed for WT and mutants. A negative ΔG indicates that a peptide is favoured for partitioning from water to lipid bilayer, so it may be suspected as fusogenic. A dash indicates that the region is no longer expected to interact with lipid bilayer and hence to be fusogenic.

Figure 2-figure supplement 2. Cell surface and intracellular detection of preS1 and preS2 HBV GP mutants. (**A, B**) Huh7 cells expressing wt or mutant HBV GPs from Figure 2 were biotinylated for 30 min at 4^{o}C and then processed biochemically. Cell lysates were subjected to streptavidin pull-down prior to western blot analysis using anti-HBsAg antibody (Murex). The molecular weight markers (kDa) are shown to the left. Calnexin detection was used as control for cytoplasm protein marker, showing the integrity of cell membrane. (**C, D**) Detection and quantification of total GP expression. Cell lysates of Huh7 cells expressing the indicated wt or mutant GPs from Figure 2 were subjected to western blot analysis using anti-HBsAg antibody (Murex). The molecular weight markers (kDa) are shown to the left. Calnexin detection was used as control for cytoplasmic protein marker, as shown in these representative western blots. The results show the relative GPs expression compared to Wt of preS1 (**C**) and preS2 mutants (**D**), as indicated, and are expressed as mean ± SD (N=3).

Figure 3-figure supplement 1. Effect of DTNB on HDV entry. Different concentrations of DTNB were added to the cell supernatant containing HDV particles at the onset of infection (0h) or at 16 hours post-infection. At 7 days post-infection virus HDV RNA from cells were extracted and quantified by RTqPCR. The results are expressed after normalization with GAPDH RNAs as means ± SD (N=3) per mL of cell lysates containing 10^6 cells.

Figure 4-figure supplement 1. Contact map prediction for the L protein by RaptorX. (**A**) The symmetric NxN matrix, where N is the length of the L protein, represents the probability of two residues being in contact. Higher probabilities are represented by darker colors. The green square highlights the “a” determinant containing the four cysteine-reach regions illustrated in Figure 4A and in (C) on the sequence. (**B**) A zoom of the green square where contacts between residues in the four cysteine-reach regions are delimited by five distinguished boxes. (**C**) Colors of the boxes pair with the links connecting the cysteine-reach regions.

Figure 4-figure supplement 2. Geometry of a disulphide bond. The five χ angles used to classify a disulfide bond conformers are labelled across the bond. MD simulations (see Methods) confirmed the stability of the bond as an allosteric disulfide, specifically on a -/+RH Hook conformation. While only three out of the twenty possible configurations, namely −RH Staple, −LH Hook and −/+RH Hook, are identified as allosteric disulfide bonds (Hogg, 2013; Schmidt and Hogg, 2007), the -/+RH Hook conformation is more stressed than other geometries, due to stretching of the S-S bond and bending of the neighboring bond angles (Zhou et al., 2014).

Figure 7-figure supplement 1. Down-regulation of PDI family members. (**A-C**) Naïve Huh7-NTCP cells (Ctrl+) or shRNA-expressing Huh7-NTCP cells were subjected to flow cytometry (left) and western blot (right) analyses, in order to evaluate the expression levels of the indicated PDIs [(A), ERp46; (B), ERp57; (C), ERp72] before or after down-regulation. Huh7-NTCP cells stained with secondary antibody only (Neg) were used to provide the background of flow cytometry analyses.

Figure 7-figure supplement 2. NTCP expression in target cells. (**A**) Huh7-NTCP and Huh7-NTCP-tat cells were subjected to flow cytometry analysis, in order to evaluate the expression of NTCP at intracellular and cell surface levels, as indicated. Cells stained with secondary antibody only (Neg) were used to provide the background of flow cytometry analyses. (**B**) Huh7-NTCP and (**C**) Huh7-NTCP-tat cells were subjected to flow cytometry analysis, in order to evaluate the expression of NTCP after the stable expression of shRNAs targeting the indicated PDIs. Non-transduced cells were used as positive control (Crtl+) and cells stained with secondary antibody only (Neg) were used to provide the background of flow cytometry analysis.

Figure 9-figure supplement 1. (**A**) NTZ at 30 µg/mL was added to the cell supernatant 2h before infection (2h-) *vs*. at the onset of infection (0h), at 4h (4h+) or at 16h (16h+) post-infection. DMSO was used as control vehicle. At 7 days post-infection, HDV RNAs were extracted from cells and quantified by RTqPCR. The results are expressed after normalization with GAPDH RNAs as means ± SD (N=4)

per mL of cell lysates containing 10^6 cells**.** (**B-E**) Study of NTZ effect in HBV *in vivo*. 4-8 weeks old NOD-FRG mice were engrafted with primary human hepatocytes (PHH). After *ca*. 2-3 months, the animals displaying HSA levels >15 mg/mL were split in 4 groups that were infected with HBV (10^8 GE/mouse) with or without NTZ. See schedule in Figure 9A. At different time points post-infection, blood samples (50 µl) were collected and the viremia in sera was monitored by qPCR on the HBV genome (GE/mL of serum) The graphs show the results of viremia for individual mice within each group. (**B**) Group #1: mice were infected and inoculated with DMSO, (**C**) Group #2: mice were infected and inoculated with NTZ (100 mg/kg), (**D**) Group #3: mice were only inoculated with NTZ (100 mg/kg) and (**E**) Group #4: mice were only inoculated with DMSO (used as control vehicle of NTZ).

Legend to Supplementary file

Supplementary file 1. Oligonucleotide sequences used for shRNAs and mutagenesis. The sequences correspond to the oligonucleotides used to generate the lentiviral vectors carrying shRNA against the indicated PDIs in Figure 7 or the HBV GP mutants described in Figure 2 (preS1 and preS2 mutants) and in Figures 4 and 5 (CSD mutants).

Legends to the source data files

Figure 1-source data 1. HBV GP fusion trigger is independent of acid pH and NTCP. The values correspond to the data expressed in the graphs displayed in Figure 1A, 1D and 1F.

Figure 1-source data 2. HBV GP fusion trigger is independent of acid pH and NTCP. These images are the original and uncropped gels that correspond to the blots displayed in Figure 1E. The vertical bars correspond to samples that were not described in the Results section.

Figure 2-source data 1. Functional analysis of predicted HBV fusion peptides. The values correspond to the data expressed in the graphs displayed in Figure 2C, 2D, 2E, 2F, 2I and 2J.

Figure 2-source data 2. Functional analysis of predicted HBV fusion peptides. The values correspond to the data expressed in the graphs displayed in Figure 2G.

Figure 2-source data 3. Functional analysis of predicted HBV fusion peptides. The values correspond to the data expressed in the graphs displayed in Figure 2H.

Figure 3-source data 1. DTNB, a thiol-specific oxidizing reagent, inhibits HBV membrane fusion. The values correspond to the data expressed in the graphs displayed in Figure 3A and 3B.

Figure 3-source data 2. DTNB, a thiol-specific oxidizing reagent, inhibits HBV membrane fusion. These images are the original and uncropped gels that correspond to the blots displayed in Figure 3C.

Figure 3-source data 3. DTNB, a thiol-specific oxidizing reagent, inhibits HBV membrane fusion. These images are the original and uncropped gels that correspond to the blots displayed in Figure 3D.

Figure 5-source data 1. Evidence for a functional role of the CSD in the region 294-317 of the HBV S GP. The values correspond to the data expressed in the graphs displayed in Figure 5A-5C.

Figure 5-source data 2. Evidence for a functional role of the CSD in the region 294-317 of the HBV S GP. The values correspond to the data expressed in the graphs displayed in Figure 5D.

Figure 5-source data 3. Evidence for a functional role of the CSD in the region 294-317 of the HBV S GP. These images are the original and uncropped gels that correspond to the blots displayed in Figure 5C. The vertical bars correspond to samples that were not described in the Results section.

Figure 6-source data 1. **PDI inhibitors in HBV entry.** The values correspond to the data expressed in the graphs displayed in Figure 6A-6D.

Figure 7-source data 1. ERp57 down-regulation inhibits in HBV entry. The values correspond to the data expressed in the graphs displayed in Figure 7B-7D.

Figure 9-source data 1. *In vivo* assessment of ERp57 inhibition. The values correspond to the data expressed in the graphs displayed in Figure 9B.

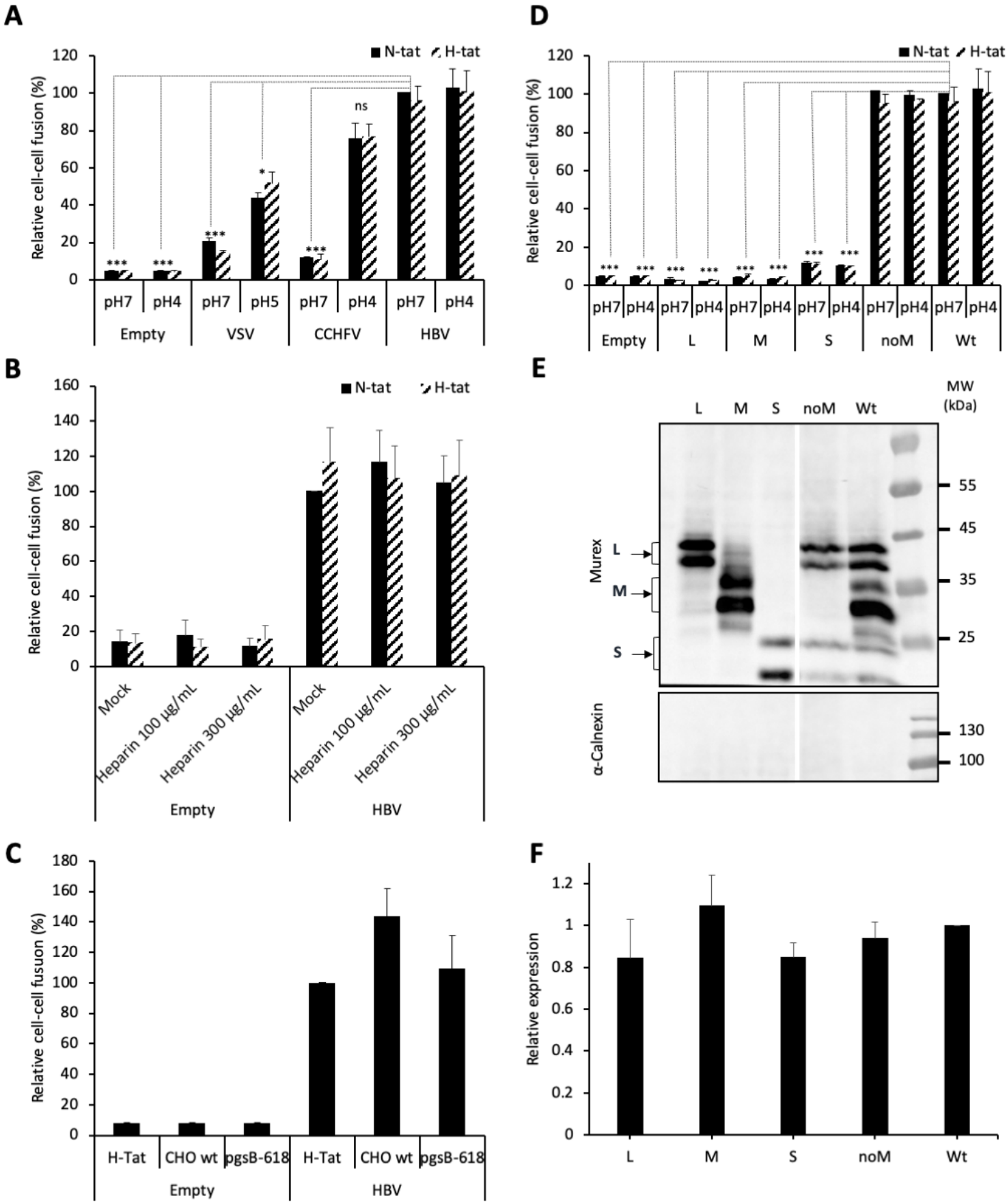

Figure 1. Pérez-Vargas et al.

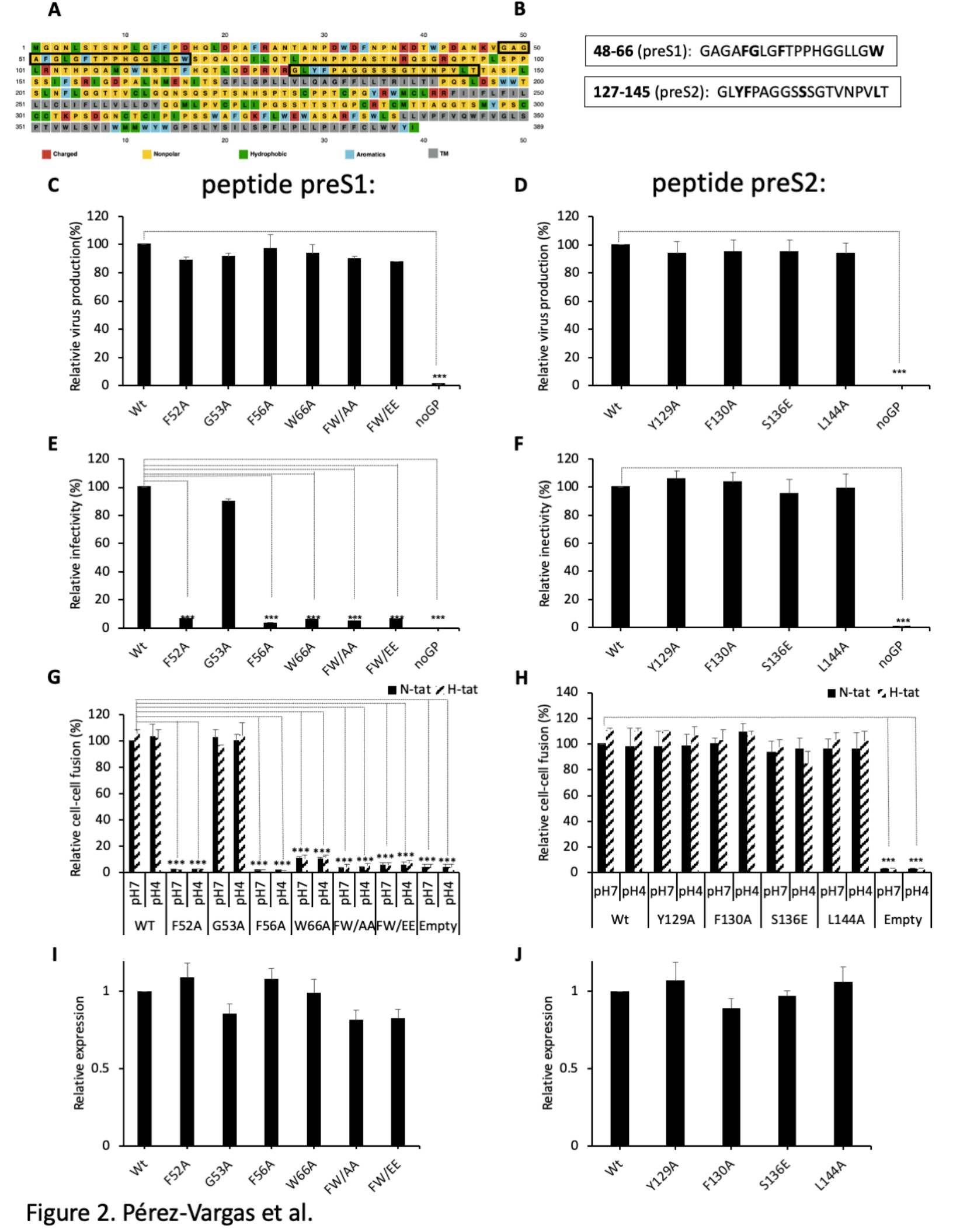

Figure 2. Pérez-Vargas et al.

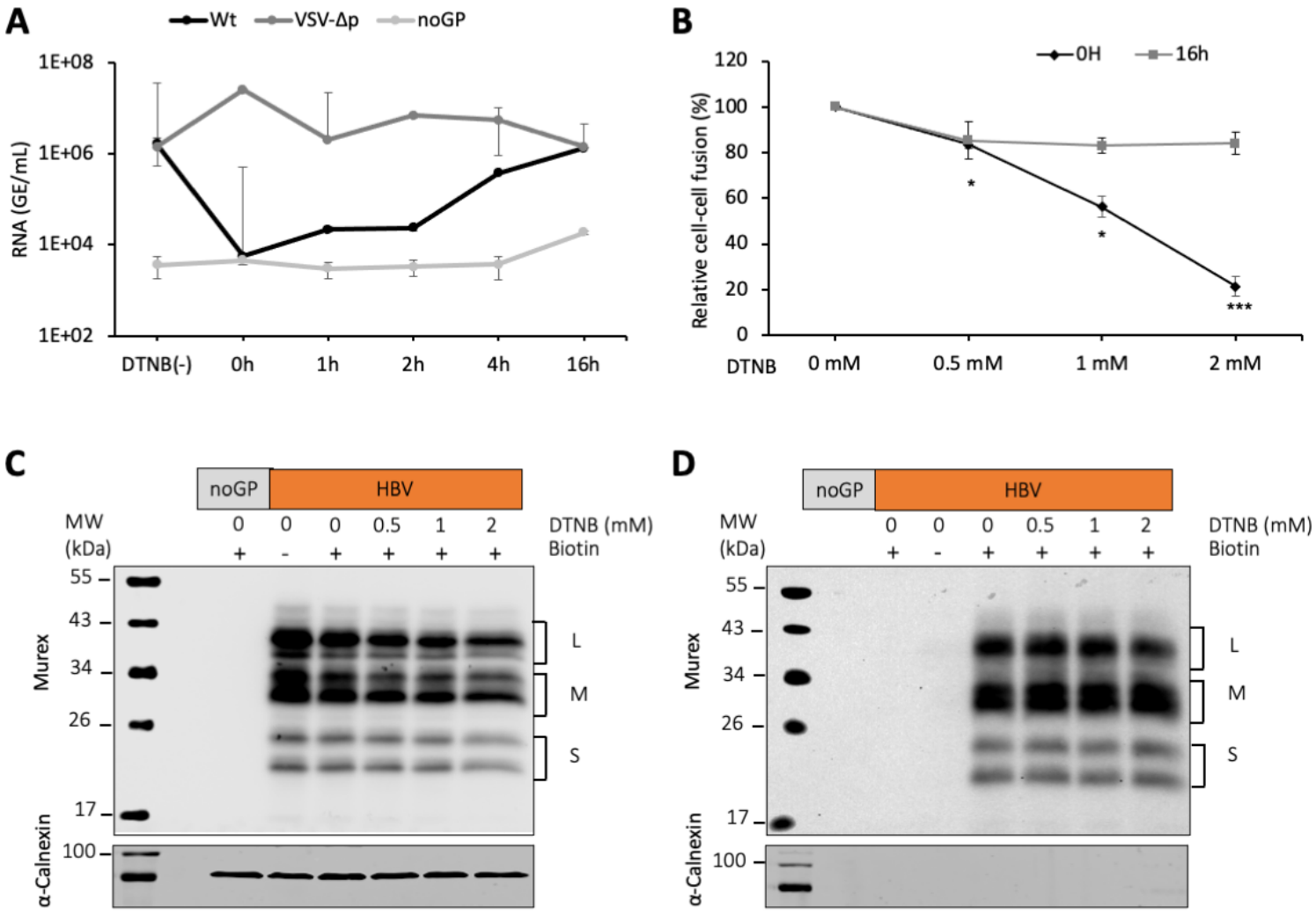

Figure 3. Pérez-Vargas et al.

A

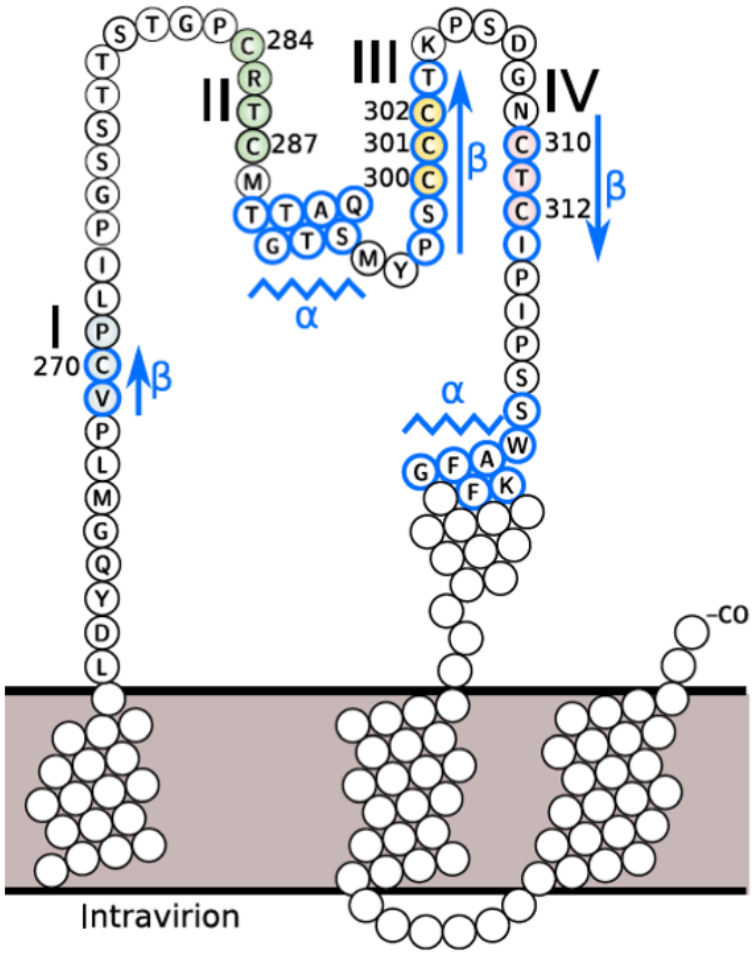

B

		II				III			IV		
		284	285	286	287	300	301	302	310	311	312
I	269	0.30	0.18	0.19	0.28	0.38	0.39	0.30	0.38	0.39	0.45
	C270	0.47	0.23	0.26	0.43	0.53	0.58	0.47	0.57	0.40	0.57
	271	0.29	0.20	0.22	0.31	0.35	0.35	0.29	0.35	0.34	0.35
II	C284					0.60	0.58	0.52	0.64	0.45	0.62
	285					0.40	0.38	0.30	0.36	0.27	0.34
	286					0.44	0.36	0.28	0.38	0.35	0.39
	C287					0.58	0.50	0.40	0.49	0.35	0.58
III	C300								0.49	0.43	**0.83**
	C301								0.62	0.54	**0.84**
	C302								**0.87**	**0.78**	**0.84**

C

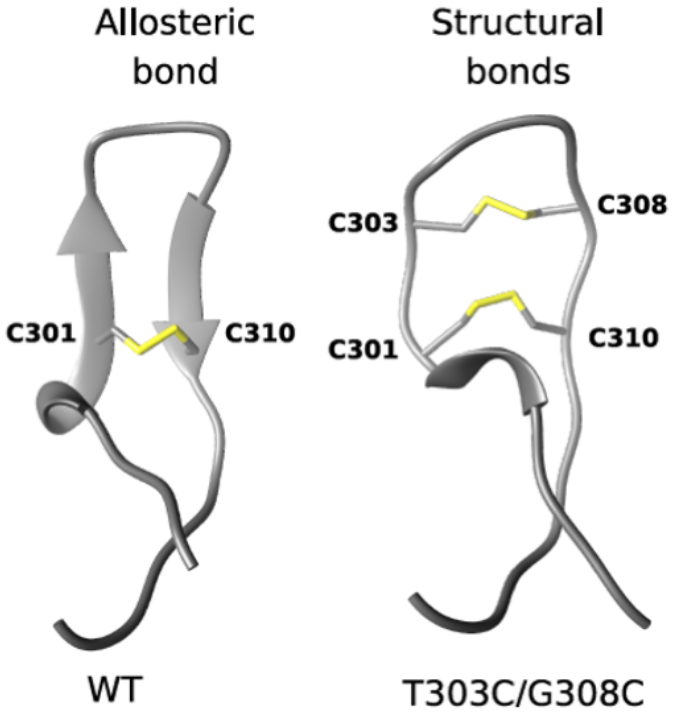

Figure 4. Pérez-Vargas et al.

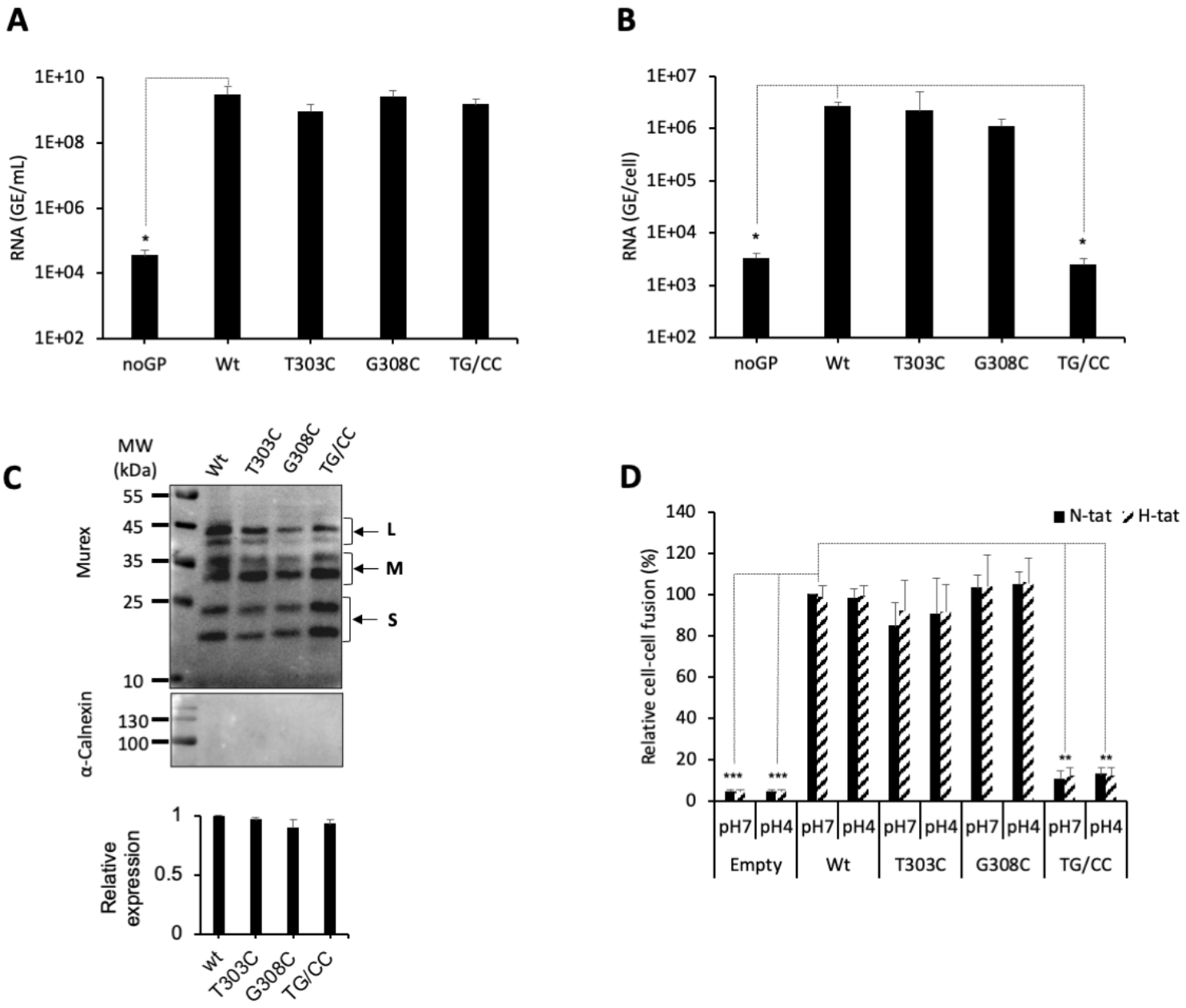

Figure 5. Pérez-Vargas et al.

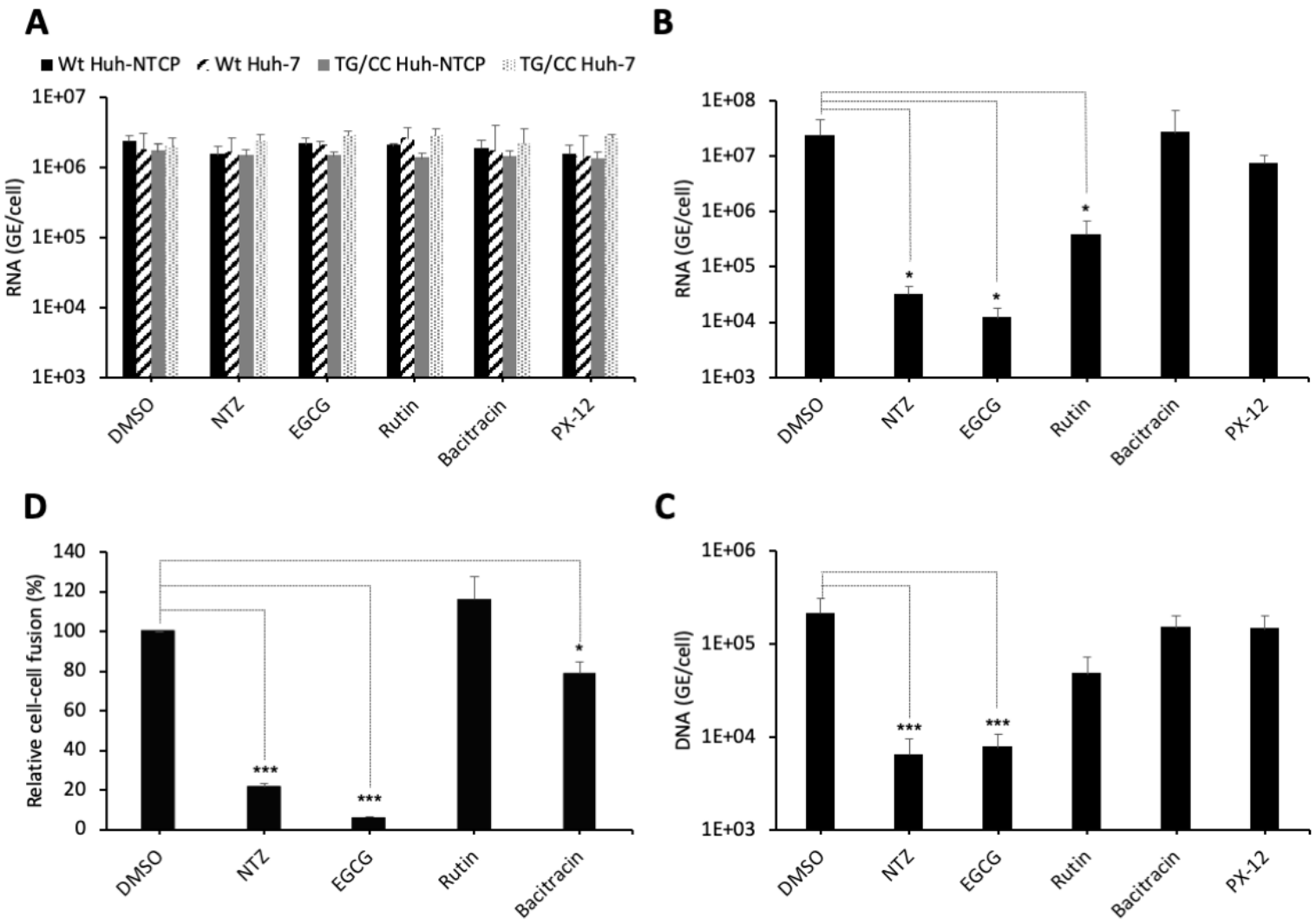

Figure 6. Pérez-Vargas et al.

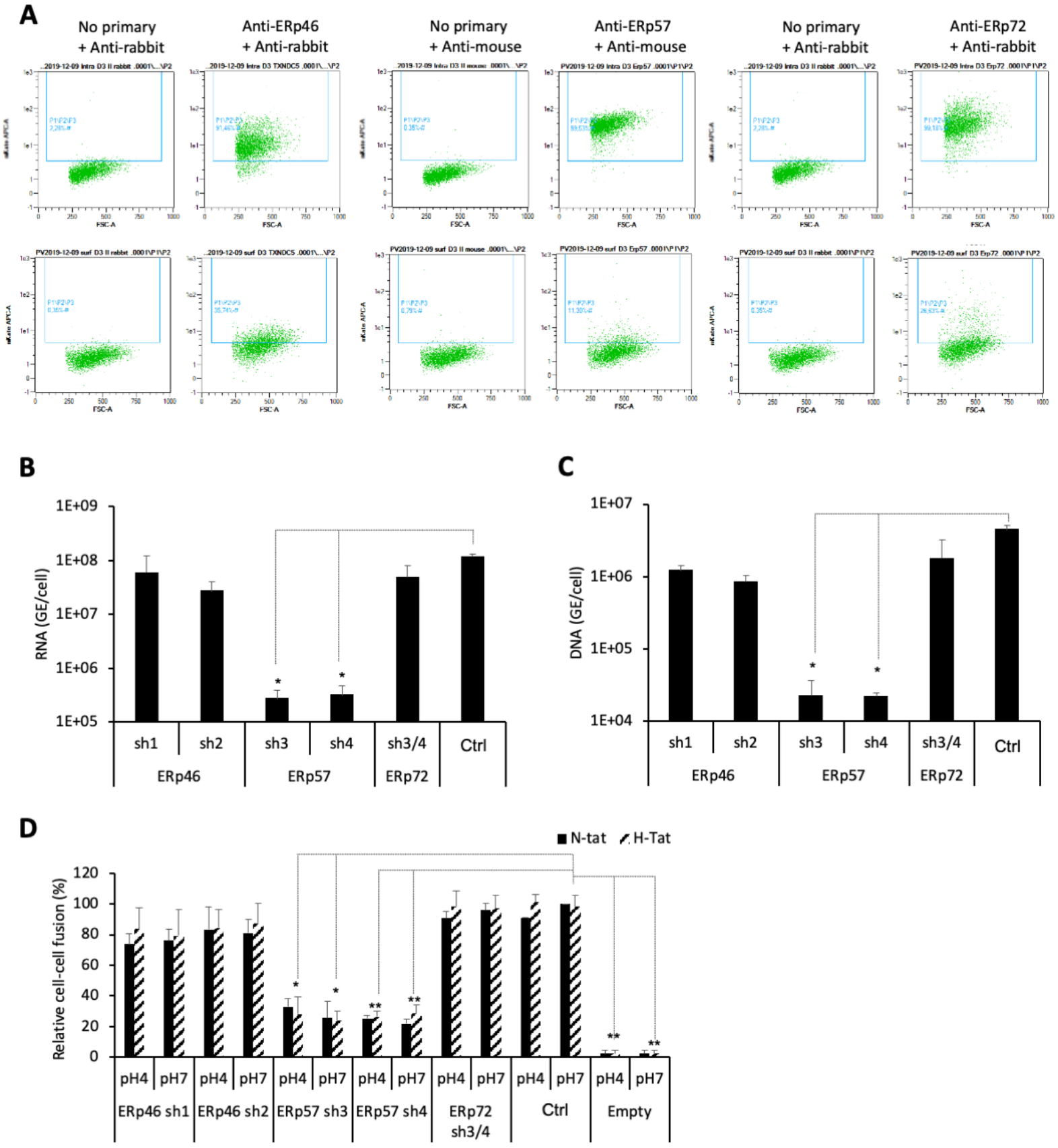

Figure 7. Pérez-Vargas et al.

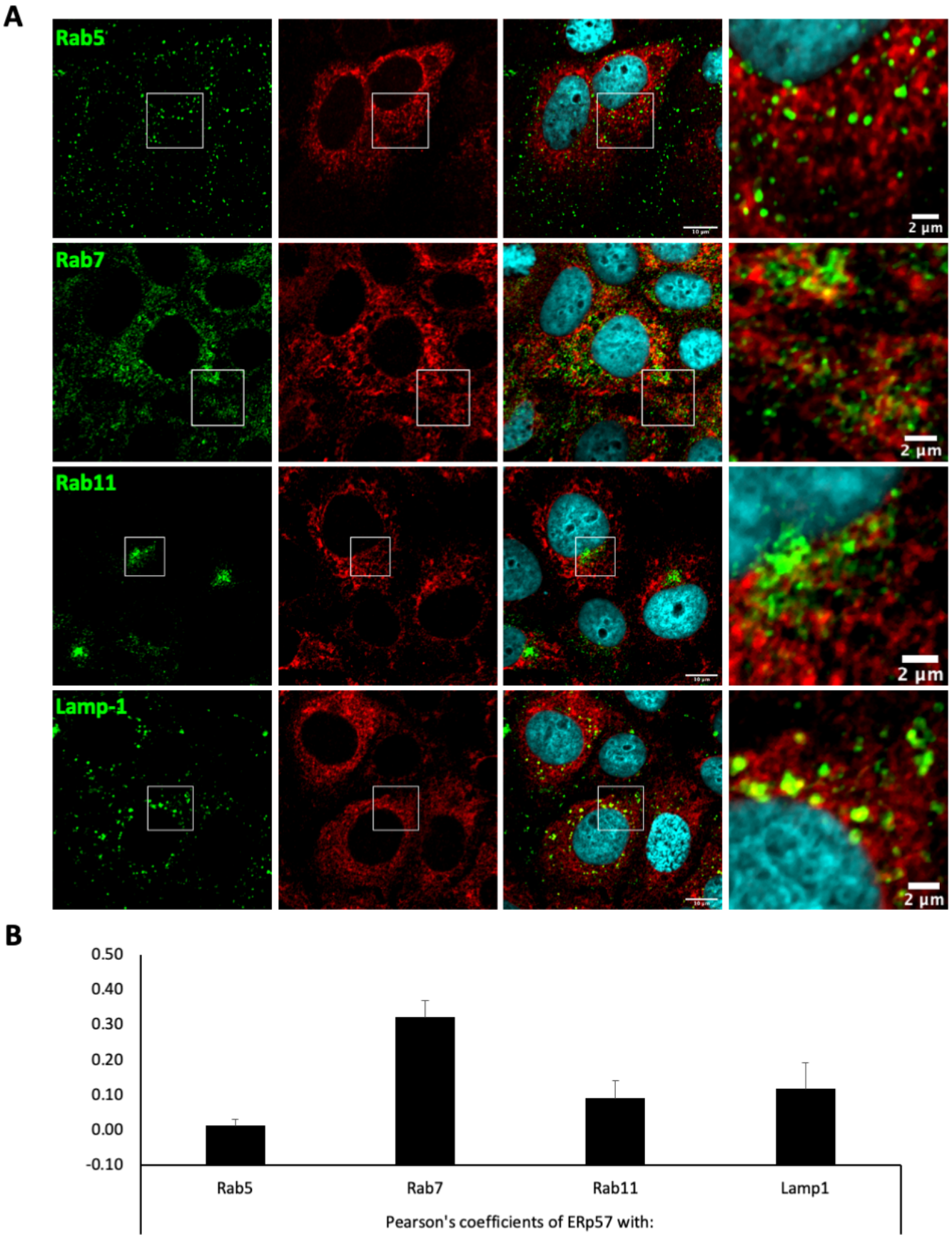

Figure 8. Pérez-Vargas et al.

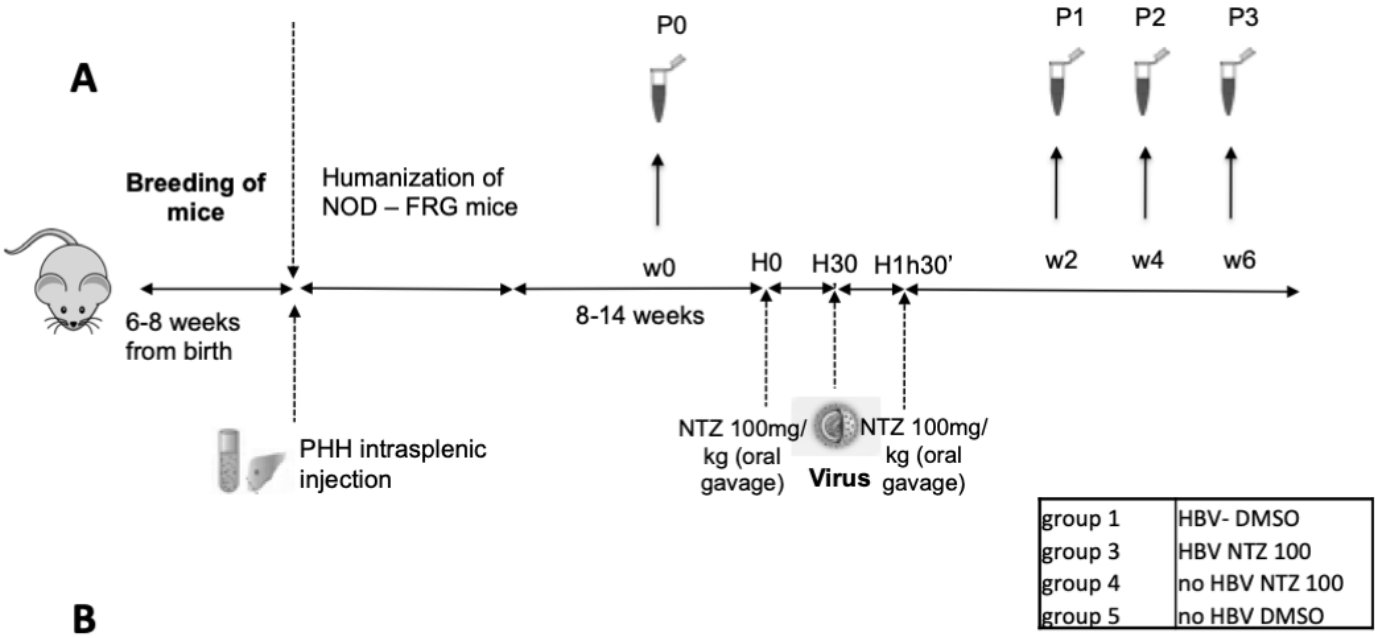

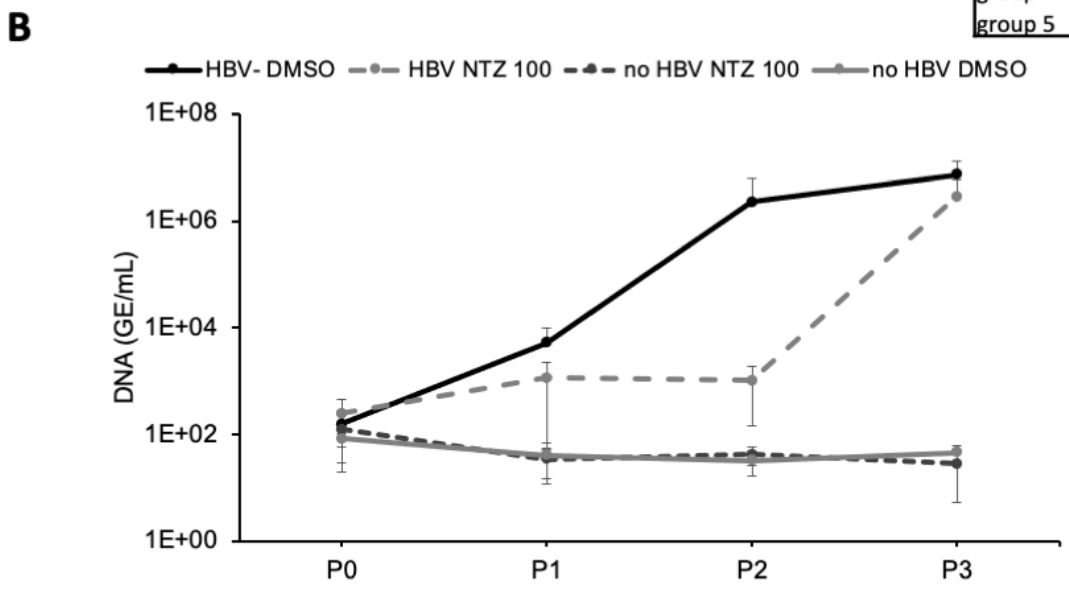

Figure 9. Pérez-Vargas et al.

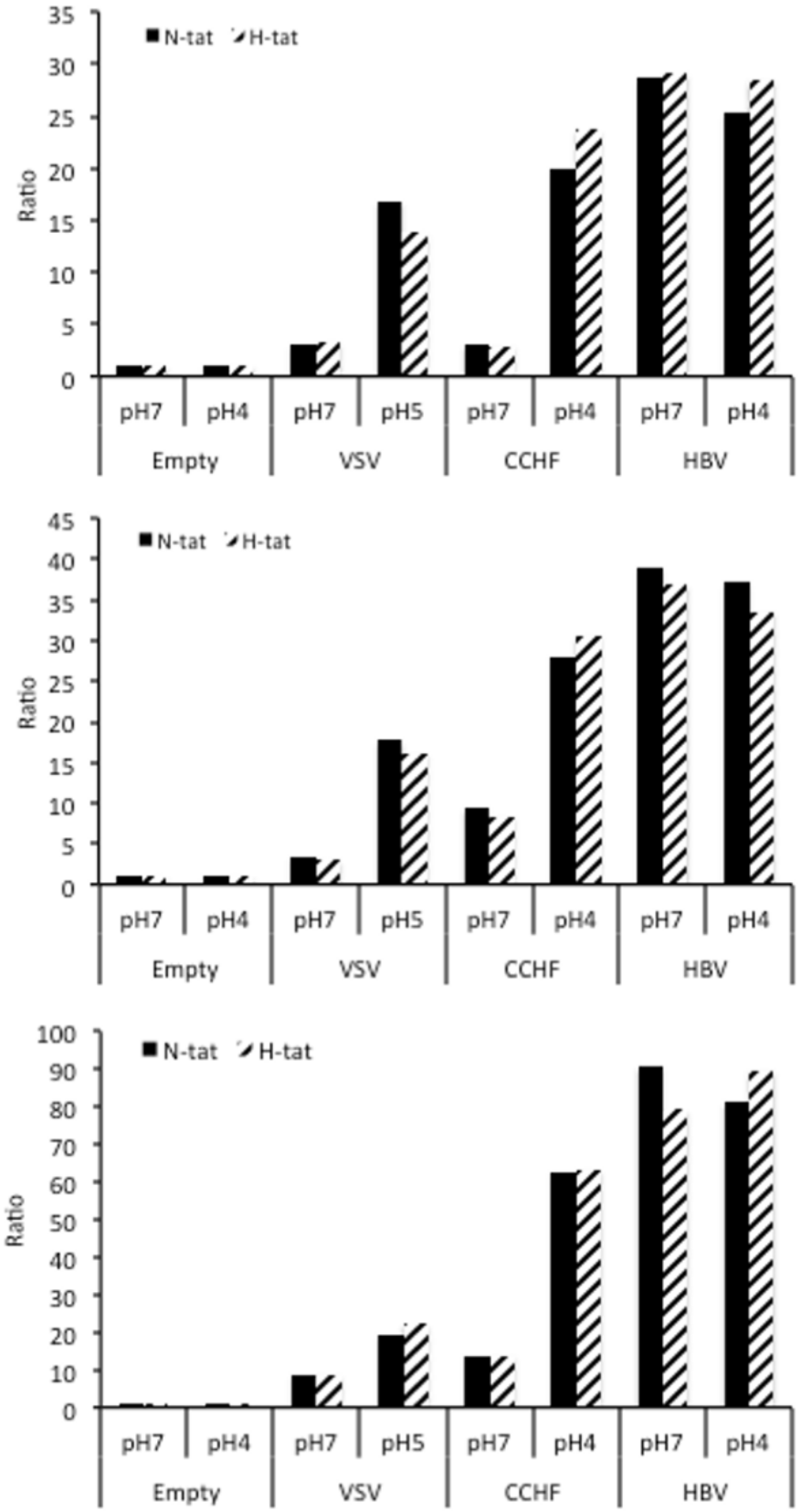

Figure 1-figure supplement 1

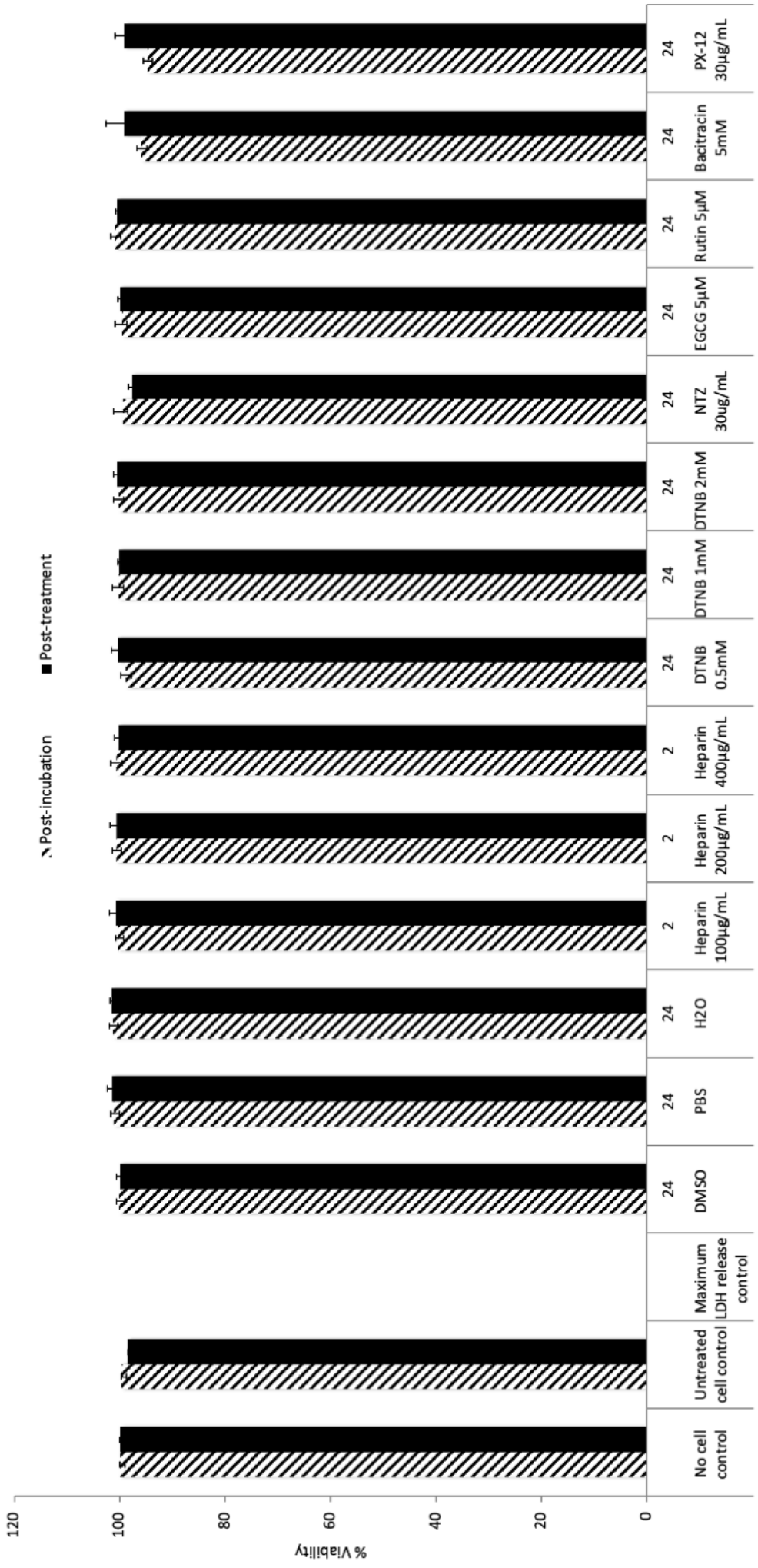

Figure 1-figure supplement 2

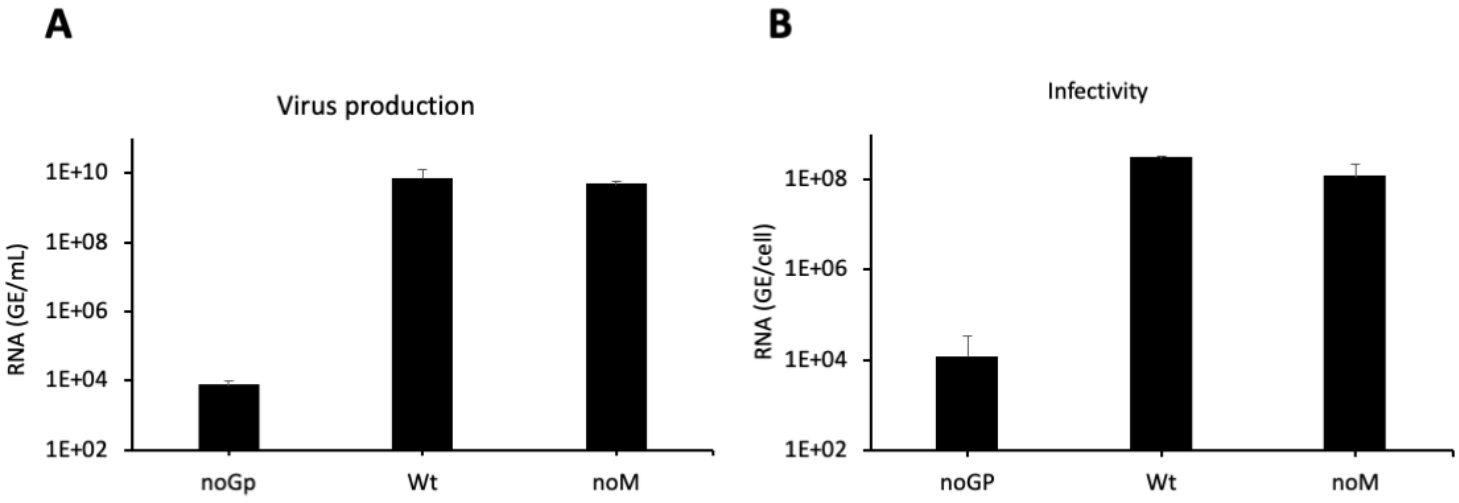

Figure 1-figure supplement 3

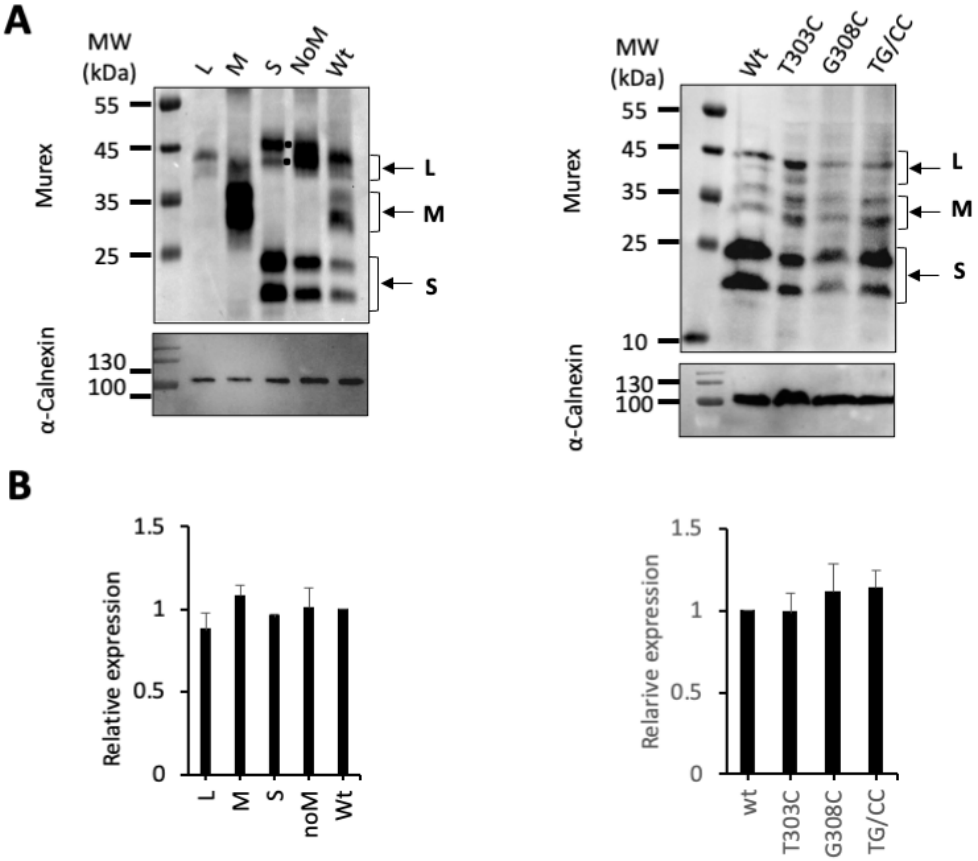

Figure 1-figure supplement 4

A

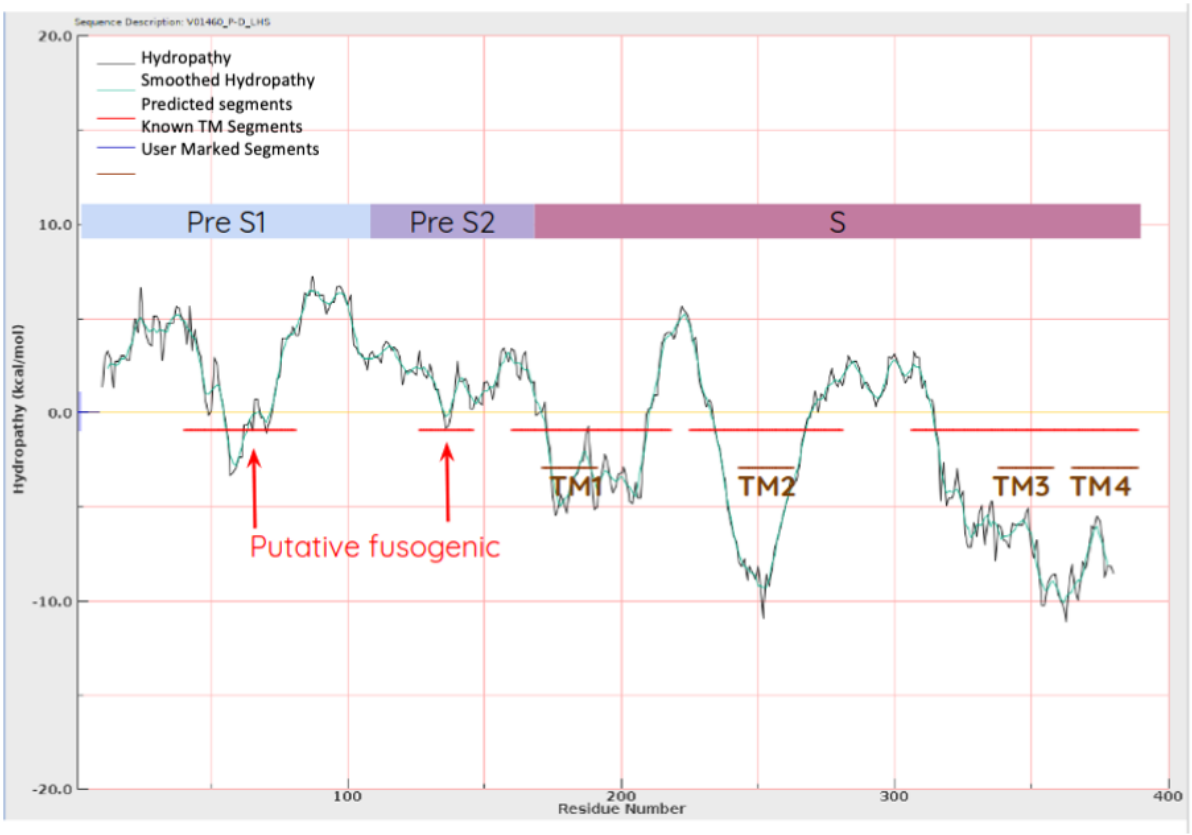

B

First fusion candidate			Second fusion candidate		
	ΔG (Kcal/mol)	Predicted region		ΔG (Kcal/mol)	Predicted region
wt	-3.38	48-66	wt	-0.85	127-145
F52A	-2.08	48-66	Y129A	-	-
G53A	-3.22	48-66	F130A	-	-
F56A	-2.08	48-66	S136E	-	-
W66A	-1.46	47-65	L144A	-0.12	127-145
F52A/W56A	-0.16	61-79			
F52E/W56E	-	-			

Figure 2-figure supplement 1

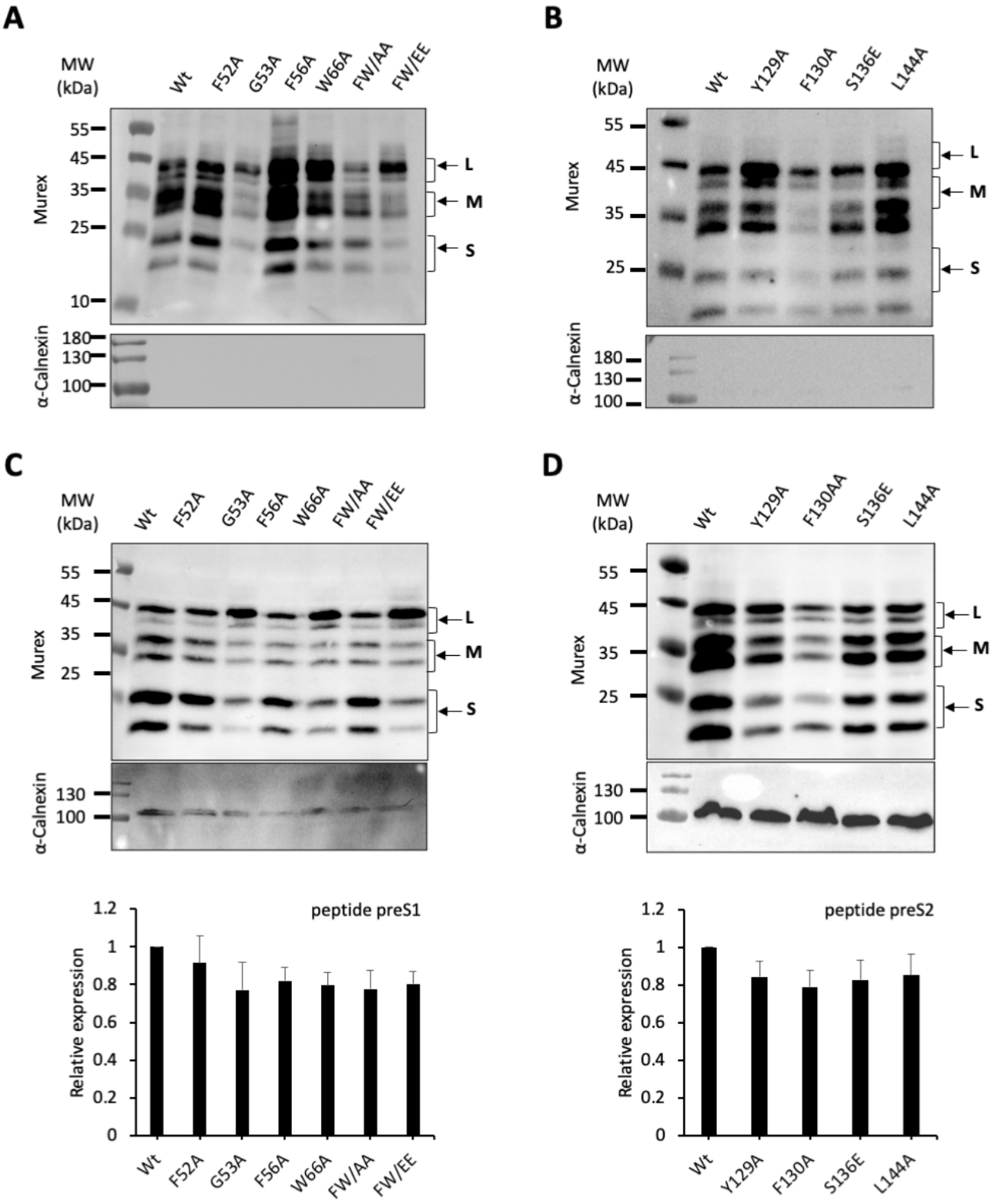

Figure 2-figure supplement 2

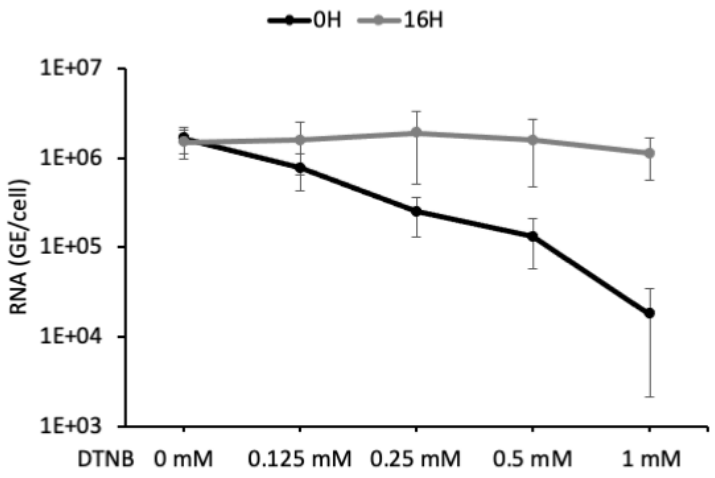

Figure 3-figure supplement 1

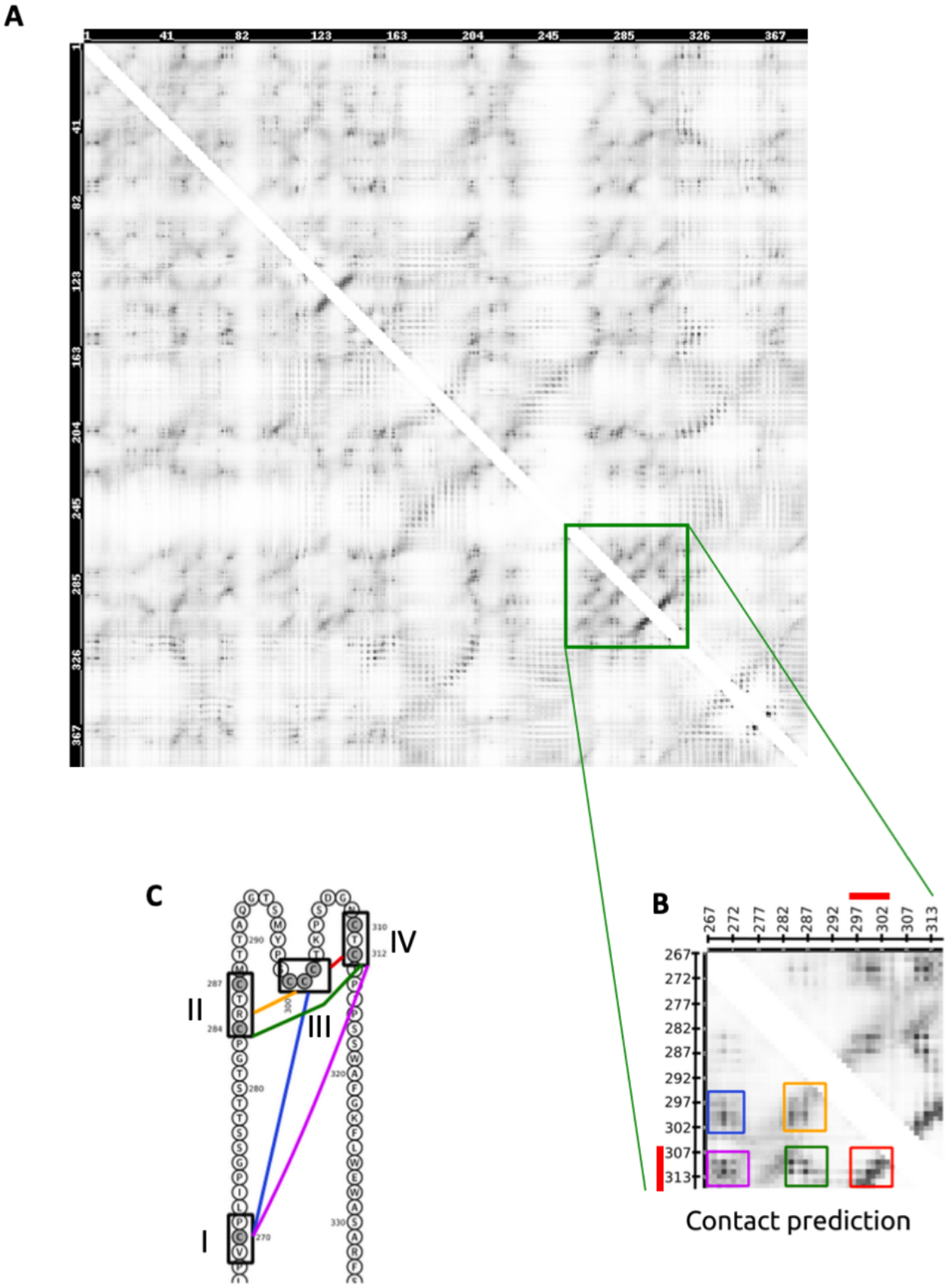

Figure 4-figure supplement 1

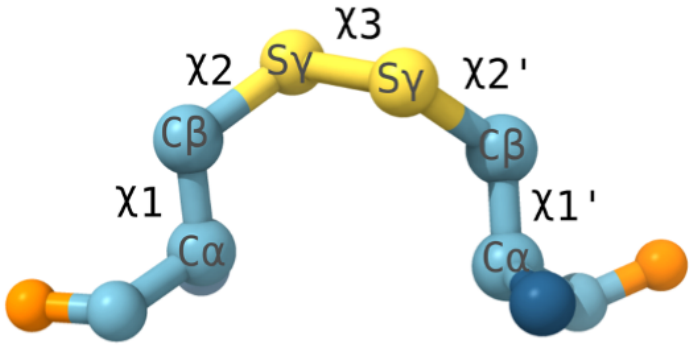

Figure 4-figure supplement 2

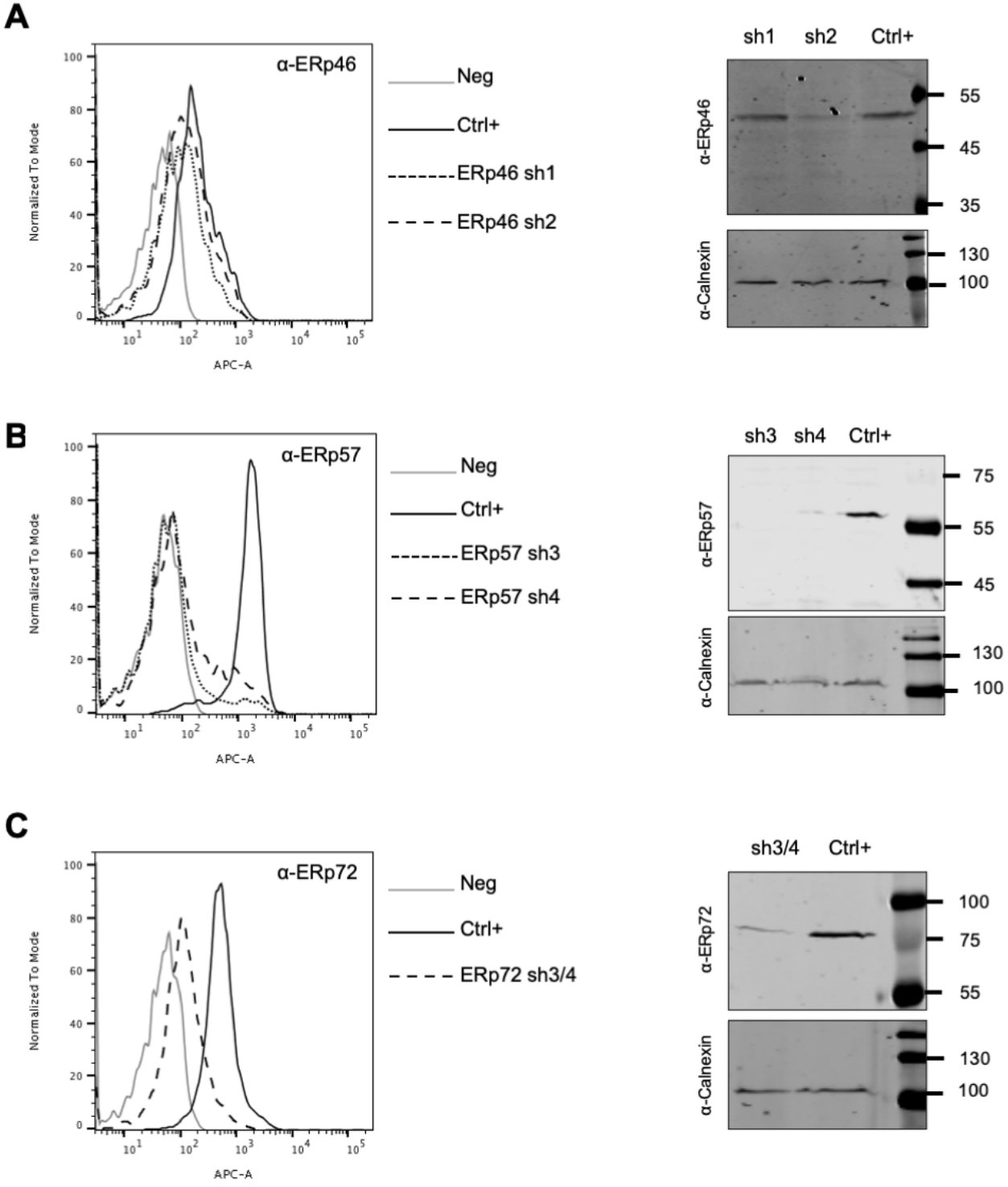

Figure 7-figure supplement 1

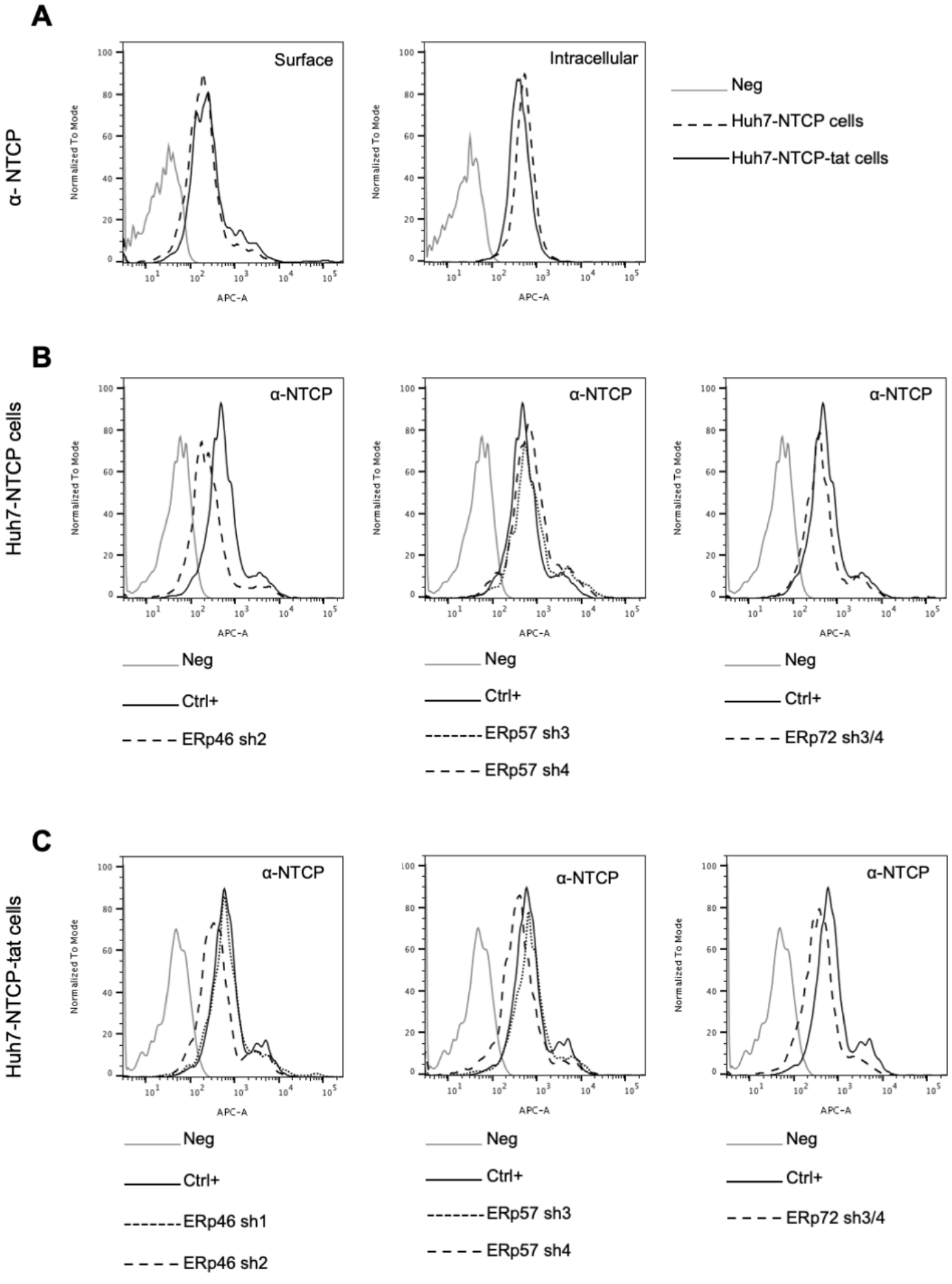

Figure 7-figure supplement 2

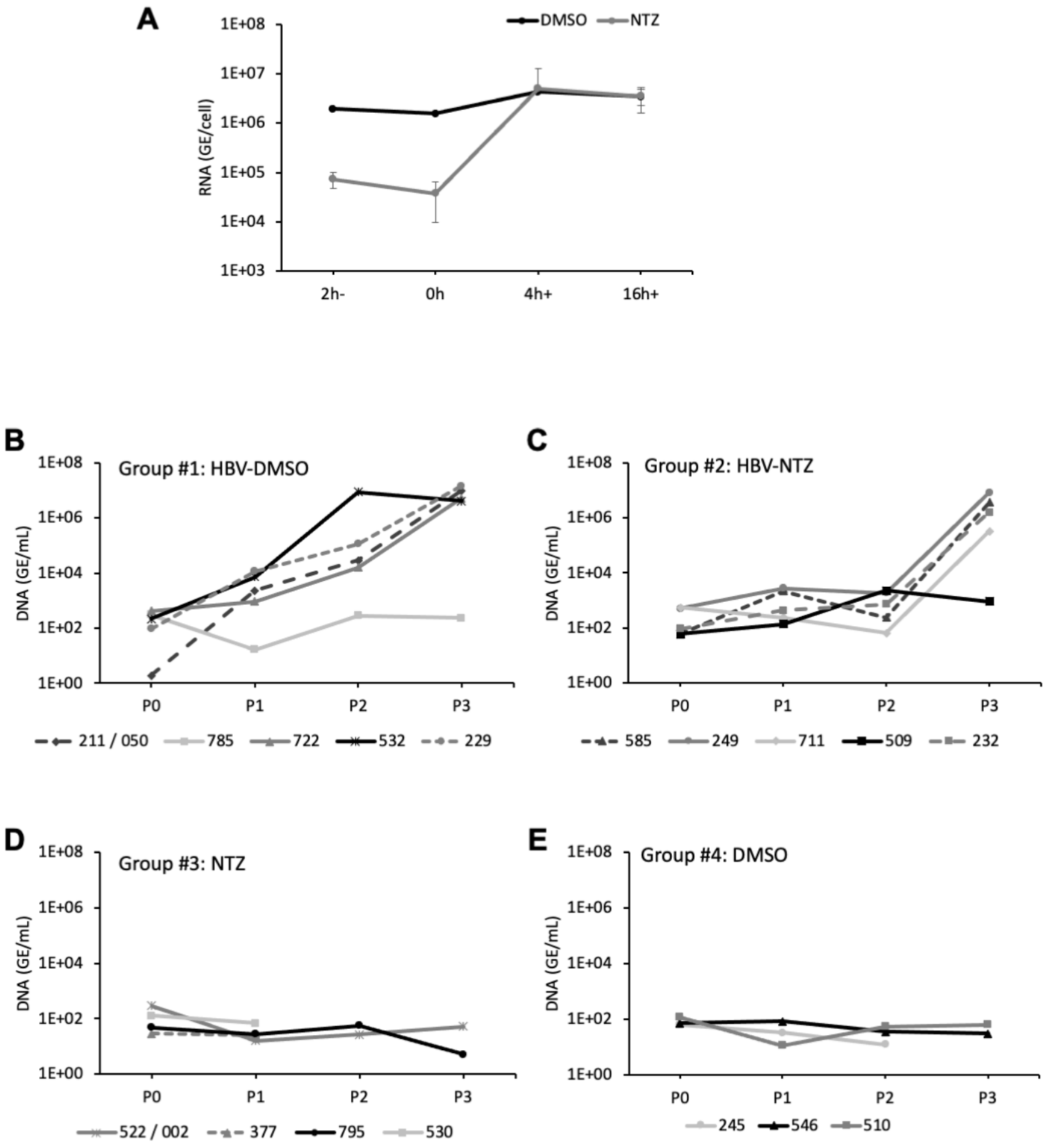

Figure 9-figure supplement 1